AR-009-682

DSTO-TR-0329

Installation-Induced Stress in a Black Hawk Inner Fuselage Panel

C.G. Knight

DEPARTMENT OF DEFENCE
DEFENCE SCIENCE AND TECHNOLOGY ORGANISATION

DISCLAIMER NOTICE

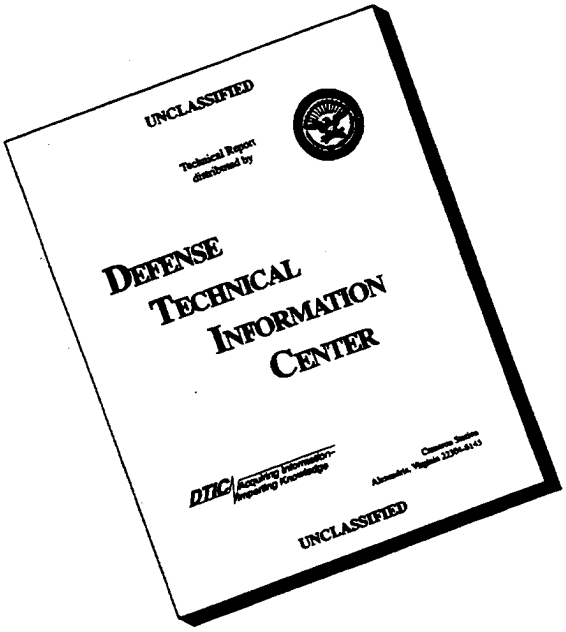

THIS DOCUMENT IS BEST QUALITY AVAILABLE. THE COPY FURNISHED TO DTIC CONTAINED A SIGNIFICANT NUMBER OF PAGES WHICH DO NOT REPRODUCE LEGIBLY.

Installation-Induced Stress in a Black Hawk Inner Fuselage Panel

C.G. Knight

Airframes and Engines Division
Aeronautical and Maritime Research Laboratory

DSTO-TR-0329

ABSTRACT

Some S-70A-9 Black Hawk helicopters of the Australian Army fleet are experiencing cracking on the starboard side internal fuselage skin panel. The panel is installed onto curved frames which causes installation-induced stresses in the panel. The PAFEC Finite Element package has been used to model the panel and to indicate the stresses and stress concentrations within it induced by the installation process.

The methods used for constructing and verifying the model are presented. The maximum stresses and stress concentration factors produced by the model are discussed.

RELEASE LIMITATION

Approved for public release

DEPARTMENT OF DEFENCE

DEFENCE SCIENCE AND TECHNOLOGY ORGANISATION

Published by

DSTO Aeronautical and Maritime Research Laboratory
PO Box 4331
Melbourne Victoria 3001

Telephone: (03) 9626 8111
Fax: (03) 9626 8999

AR No. AR-009-682
May 1996

APPROVED FOR PUBLIC RELEASE

Installation-Induced Stress in a Black Hawk Inner Fuselage Panel

Executive Summary

Some S-70A-9 Black Hawk helicopters of the Australian Army are experiencing cracking on a starboard side internal fuselage skin panel which is riveted to fuselage frames FS295 and FS308.

Frames FS295 and FS308 are curved and the panel is brought into its final position by hand pressure. The aircraft drawings do not indicate that any stress-relieving process is applied to the panel after installation. Thus forcing the panel into the correct shape causes installation-induced stresses in it.

This report details the calculation of the installation-induced stress in the panel by a finite element (FE) analysis. The PAFEC FE analysis package was used to create the FE model and perform the calculations.

Inspection of the plots of the stress field on the panel indicate the top of the beads have a zero stress field and can thus be considered as acting like gaps in the structure. These zero stress fields create local stress concentration factors of up to 2.3.

The maximum panel installation-induced stress was calculated to be 140 MPa. Since the panel is made of an aluminium alloy with a typical yield stress of 300 MPa, the installation-induced stress represents a significant proportion of the yield stress.

The results obtained indicate a maximum stress concentration occurs on the fifth bead from the top on the aft edge of the panel and this correlates well with known crack locations on in-service Black Hawks.

The installation-induced stress is only one part of the stress applied to the panel. The panel is undergoing a complex loading pattern consisting of a variety of vibratory loads as well as significant loads from the side force and lift of the tail rotor. The panel is also mounted on the two forward lift frames and these alone exhibit a complex loading pattern.

Author

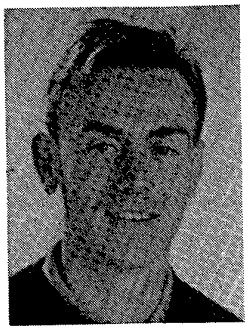

Mr C. G. Knight
Airframes and Engines Division

Mr Chris Knight is a Professional Officer in the Airframes and Engines Division at AMRL. He joined AMRL in 1994 after graduating from the University of New South Wales with an honours degree in Aerospace Engineering. He has worked in helicopter life assessment and was involved in the Black Hawk panel cracking investigation.

Contents

Abbreviation and Definitions

AMRL	Aeronautical and Maritime Research Laboratory
ARDU	Aircraft Research and Development Unit
DSTO	Defence Science and Technology Organisation
ESSS	External Stores Support System
FE	Finite Element
PAFEC	Finite Element Package
PIGS	PAFEC Interactive Graphics System
STA	Fuselage Station
WL	Water Line

1. Introduction

Some S-70A-9 Black Hawk helicopters of the Australian Army fleet are experiencing cracking on the starboard side internal fuselage skin panel that lies between fuselage frames FS295 and FS308. The cause of the cracking is currently being studied. However, one aspect of this may be the installation-induced stress within the panel.

The location of the panel is shown in Fig. 1(a), while Figs 1(b) and 1(c) show the beads pressed into the panel to provide out-of-plane stiffness. The panel is stress relieved after the beads are pressed into it and hence any installation-induced stress, due to forming the beads, is removed. However when the panel is installed in the aircraft, it must be curved to conform with the shape of frames FS295 and FS308. According to the aircraft installation drawing for the panel[1], the panel is to be "brought into installed shape by hand pressure" and then riveted to the frames. The curvature will then give rise to installation-induced stresses in the panel. These stresses will be both tensile and compressive.

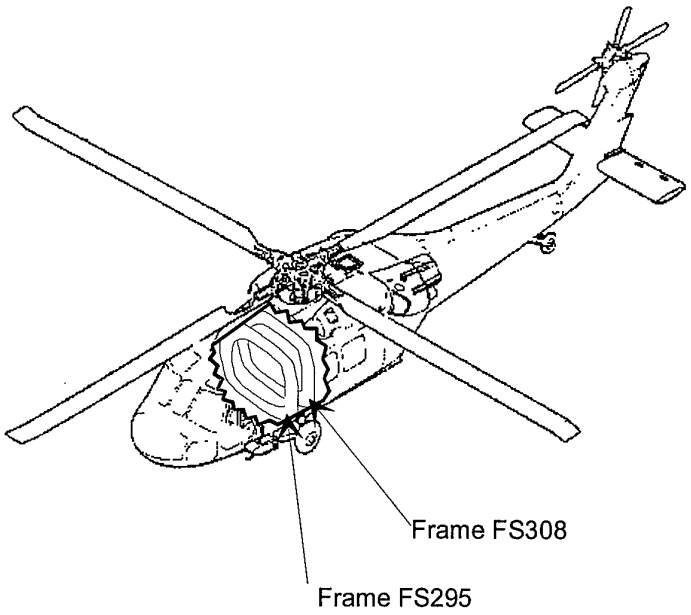

Figure 1a. Location of Frames FS295 and FS308

[1] Sikorsky Drawing Number 70219 - 02130 Fitting Assy., Upper Fus. - STA308.00

Compressive installation-induced stresses on the surface of the panel would generally be considered to be desirable as they give the component a higher resistance to fatigue damage. Tensile installation-induced stresses would generally be considered undesirable as they lower the fatigue life and fracture strength of the component. In the panel under consideration, the curvature is such that the installation-induced stresses would tend to be compressive on the inside (that is the side seen from inside the aircraft) and tensile on the outside.

However the panel is subjected to a complex load pattern. The stresses in the panel come from the vibratory load induced by the main rotor and tail rotor. In addition there are stresses due to the side force of the tail rotor (which leads to bending, lifting and twisting moments). Thus the installation-induced stresses calculated in this report are only a part of the stresses that the panel is subjected to.

Due to the complex shape of the panel a finite element (FE) package (PAFEC) was used to model the panel. This report outlines the method and results of the finite element analysis of the panel.

A shell type element has been used and the validity of using this element was verified by comparing the results that the element produced for a cantilevered beam against the analytical results for a cantilevered beam.

The analysis of the panel was based on applying displacements to the FE model elements so that the FE model took up the correct curved shape. This type of analysis was verified by calculating the results obtained by applying displacements to an FE model of a flat plate and comparing the resulting stresses with those obtained from an analytical analysis.

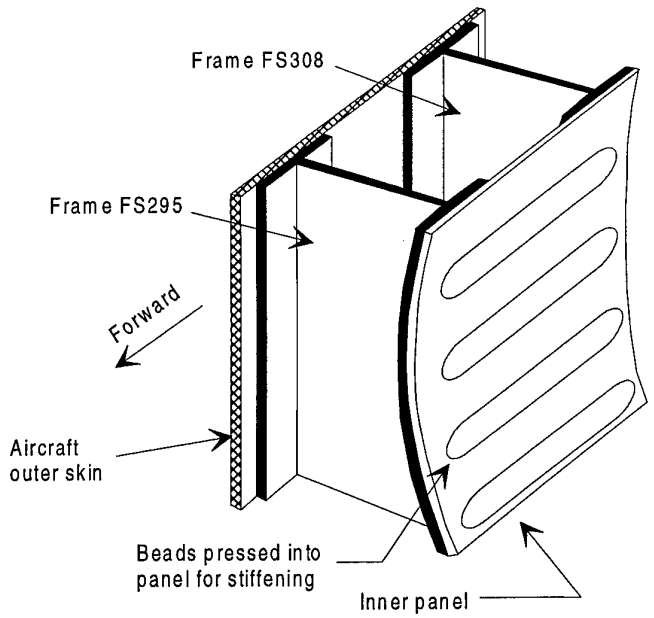

Figure 1b. Close-up View of the Panel

Due to the curvature of the beads, triangular elements were required for the model, but triangular elements are known to be significantly inferior to quadrilateral elements. However the use of some in-house code generators has allowed the use of triangular elements in the model such that the results are predictable. In addition, the triangular elements are located in lowly stressed parts of the panel.

Plots of the Von Mises stress fields and the lengthwise fibre stresses on both the inner and outer surface are provided. As well, comparison of the results with existing crack location information is presented and some conclusions drawn concerning the effect of the beads with regard to the installation-induced stress field.

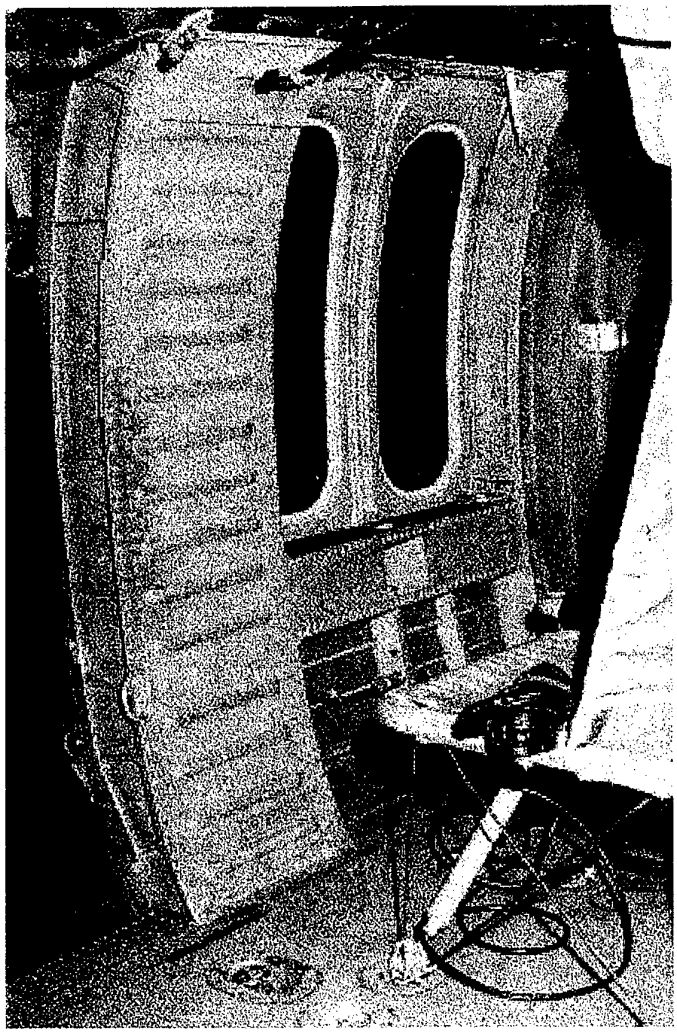

Figure 1c. Left Side Fuselage Panel

2. Fuselage Inner Panel

After the element type (43210) and the prescribed-displacement method had been validated with simple comparisons of analytical and finite element solutions (Appendices A, B and C), the actual panel could be constructed as a finite element array.

Due to the presence of a doubler on the aft edge and not on the forward edge of the panel, symmetry could not be used to model the panel. To save on model size, only four and a half beads were modelled and the prescribed displacements were transposed down one bead to represent a second section of the overall panel. The modelled panel section is shown in Fig. 2.

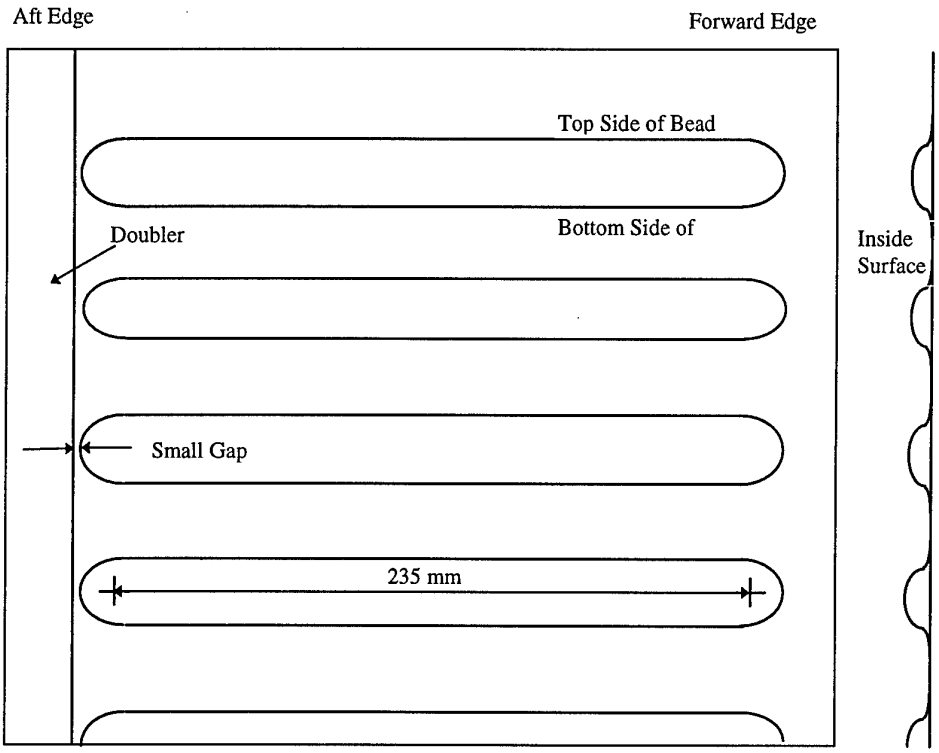

Figure 2. Extent of the Panel Section Modelled.

The panel dimensions were obtained from the relevant aircraft drawings and supplemented by measurements of the panel on aircraft A25-206. The measured panel was found to be 384.05 mm wide and 0.05" (1.27 mm) thick. The area of analysis extends from WL238.606 to WL257.000 and is 330.2 mm wide. The area of analysis is not as wide as the actual panel because the prescribed-displacement method only requires the panel between the centre lines of the two rows of rivets to be modelled and this decreased the model size.

The beads were found to be 5 mm deep with a major radius of 12.5 mm and a washout radius (recurve) of 7.9 mm (Fig. 3). The length of the bead was determined to be 235 mm between end centres.

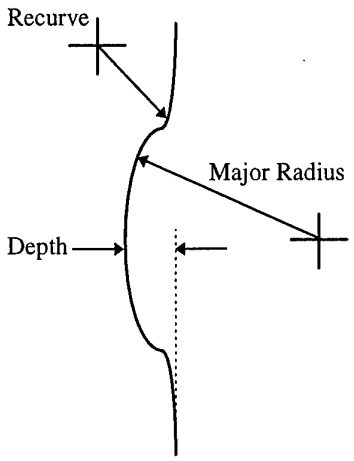

Figure 3. Detail of Panel Beading.

2.1 Finite Element Analysis

Construction of the model within PAFEC was a complex task as the dual curvature of the bead required additional input for mid-side nodes. The positions of all major nodes were calculated analytically and input directly into the data file.

The first model consisted of one quarter of one bead as shown in Fig. 4. Initially a problem was found in the runout of the bead where it met the forward edge of the doubler. The use of triangular elements were required in this region.

The PAFEC manual (Ref. 1) states in section 4.56 that:

> *"the six noded triangular element is very inferior to the quadrilateral element. The quadrilateral should be chosen whenever possible."*

However, inspection of the aircraft indicated a small gap of 1.5 mm between these points as shown in Fig. 2. This gap allowed quadrilateral elements to replace the triangular elements at these positions.

The six noded triangular elements (43110) were still required for use at the centre end of the bead. An initial test run of the quarter bead model indicated serious discontinuities at the positions containing the triangular elements. The triangular elements were replaced by an element produced from existing PAFEC pafblocks utilising an in-house data generator.

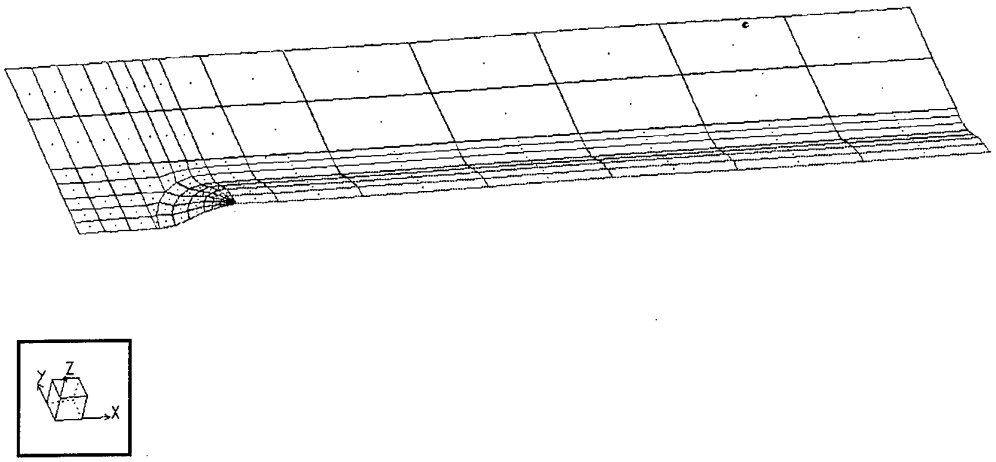

Figure 4. Quarter Bead Model Mesh.

This reduced the number of triangular elements and limited their use to the ends of the beads close to the top where the stresses were known to be very small. The panel was then analysed and found to give adequate results in the area of concern.

The full model was produced from this quarter-bead model by copying and mirror imaging the model as necessary. The full model is shown in Fig. 5.

After the model had been constructed within PAFEC it was necessary to find data to generate the shape of the curve. Information from Sikorsky Drawing Number 70219-02130 ***Fitting Assy., Upper Fus - STA 308.00,*** is included in this report as Appendix D. This drawing contains information concerning the shape of the fuselage at the frame position upon which the panel is mounted. Additional information was scaled from Sikorsky Drawing Number 70211-02107 sht 1, rev J ***Frame Instl, Upper Fus - STA 308.00.***

This curve information was entered into the plotting program ORIGIN v2.94 and a ninth order polynomial was generated to represent the panel curvature from WL 237.00 to WL 255.998. The output from this program is shown in Table 1.

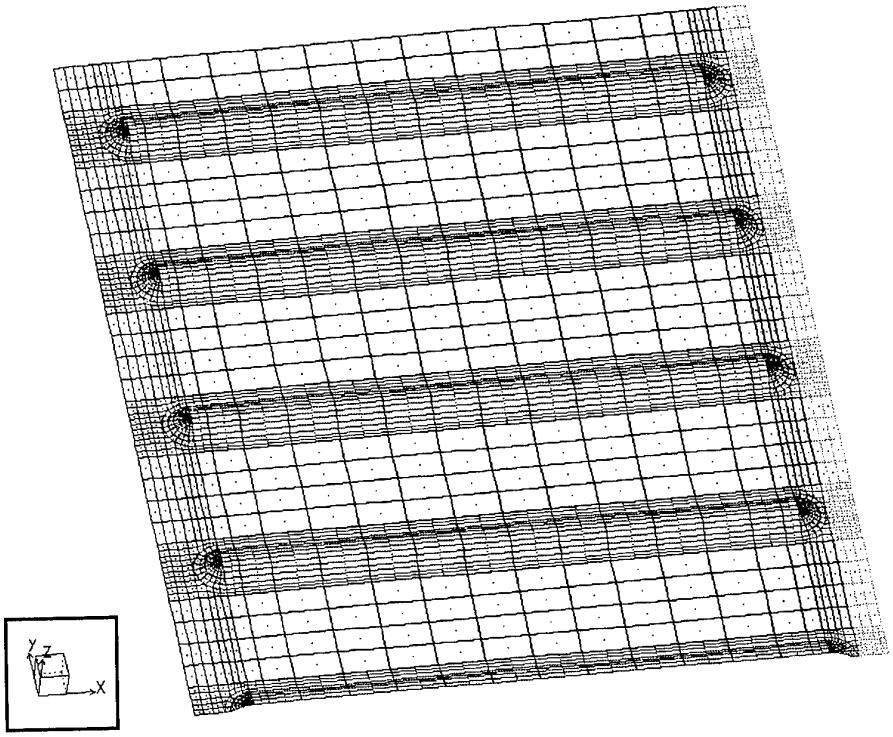

Figure 5. Full Panel Model Mesh.

Table 1. Polynomial coefficients and fitting results.

Coefficient	Value
A0	5.2840690E-03
A1	6.516517E-03
A2	2.409318E-03
A3	-4.4587075E-05
A4	4.3324607E-07
A5	-2.3362276E-09
A6	7.4562034E-12
A7	-1.4011089E-14
A8	1.4344937E-17
A9	-6.1747794E-21
Coefficient of Regression, R	1
R^2	1
Standard Deviation	0.08298

This information represents a polynomial of the form:

$$z = A_0 + A_2 y^2 + A_3 y^3 + ... + A_9 y^9$$

where y is the distance up the panel in mm and z is the distance the panel is deflected out, once again in mm.

It was found that the high number of significant figures, shown for the coefficients in Table 1, was needed to accurately replicate the original input information.

This polynomial is used, along with the information obtained from the aircraft drawings, to generate two more polynomials to represent the prescribed displacements of two sections of the overall panel. That information appears later in this section.

Appendices A and C of this report indicated that the FE model results would suffer from end effects due to the inability to properly represent the boundary conditions. For this reason results from the top bead and the bottom half-bead are ignored.

To keep the FE model to a reasonable size the region of analysis is covered by two panels each offset from each other by one bead. Where the panels overlap the results are compared for consistency.

For the purpose of this section Panel 1 is defined as the section of the overall panel extending from WL 242.944 to WL 257.000. Panel 2 is the section extending from WL 238.606 to WL 252.245.

2.1.1 Panel 1

Panel 1 is the section of the overall panel running from WL 242.944 to WL 257.0. To generate the polynomial for this section the origin of the original equation needs to be moved from WL 237.0 to WL 242.944 (ie. 5.944 inches). In consistent units for the equation this is a distance of y = 150.98 mm. The previous polynomial will generate a z value of 11.170 mm. That is, the origin of the polynomial used for Panel 1 is 150.98 mm higher and 11.70 mm further out than the origin for the polynomial given in the previous section.

These two values were then subtracted from the original data and this new information was entered into the plotting program ORIGIN v2.94 and a new ninth order polynomial was generated to represent the curve from WL 242.944 to WL 255.998. The output from this program is shown in Table 2.

Table 2. Polynomial coefficients and fitting results for Panel 1.

Coefficient	Value
A0	2.2894991E-02
A1	1.2343641E-01
A2	1.9044633E-04
A3	4.3779643E-06
A4	-5.4923672E-08
A5	4.3551560E-10
A6	-2.0482587E-12
A7	5.7075019E-15
A8	-8.6706320E-18
A9	5.5495271E-21
Coefficient of Regression, R	1
R2	1
Standard Deviation	0.01885

Again this information represents a polynomial of the form:

$$z = A_0 + A_2 y^2 + A_3 y^3 + \ldots + A_9 y^9$$

where y is the distance up the panel in mm and z is the distance the panel is deflected out, once again in mm.

Panel 1 also extends into a curve represented by a circle (see drawing number 70219-02130, Appendix D). This can be represented by the equation:

$$z = 318.1057471 - \sqrt{254.013^2 - (y - 204.6224)^2}$$

Once again this number of significant figures was necessary to accurately reflect the input information.

The two functions of y represented by these two equations coincide at WL 255.998 where y = 331.5716 mm and z = 98.091 mm.

These two equations were inserted into a simple FORTRAN routine which interfaced with a data capturing and analysis program that allowed the collection of information on aspects of the PAFEC model. Information was gathered on the y-axis coordinate of the two vertical rivet lines on each side of the panel (ie. four rows in total). This information was fed into the FORTRAN routine and the movement in the z-axis calculated based on the above equations. The information was then entered into the prescribed-displacement module of the PAFEC model.

2.1.2 Panel 2

Panel 2 is the section of the overall panel running from WL 238.606 to WL 252.245. To generate the polynomial for this section the origin of the original equation needs to be moved from WL 237.0 to WL 238.606 (ie. 1.606 inches). In consistent terms for the equation this is a distance of y = 40.80 mm. The polynomial for the whole panel will generate a z value of 2.2218 mm at y = 40.80 mm.

These two values were then subtracted from the original data and this new information was entered into the plotting program ORIGIN v2.94 and another ninth order polynomial was generated to represent the curve from WL 238.606 to WL 252.245. The output from this program is shown in Table 3.

Table 3. Polynomial coefficients and fitting results for Panel 2.

Coefficient	Value
A0	-6.1025914E-02
A1	7.949107E-02
A2	-3.2983782E-04
A3	3.8712292E-07
A4	7.9701523E-08
A5	-8.0767058E-10
A6	3.7351987E-12
A7	-9.2102501E-15
A8	1.1760002E-17
A9	-6.1212384E-21
Coefficient of Regression, R	1
R^2	1
Standard Deviation	0.08303

Again this information represents a polynomial of the form:

$$z = A_0 + A_2 y^2 + A_3 y^3 + \ldots + A_9 y^9$$

where y is the distance up the panel in mm and z is the distance the panel is deflected in mm.

Once again these two equations were inserted into a simple FORTRAN routine. Information was gathered on the y-axis coordinate of the two vertical rivet lines on each side of the panel (ie. four rows in total). This information was used to calculate the z-axis based on the above equations. The information was then entered into the prescribed-displacement module of the PAFEC model.

2.2 Results

Both panel models were run with the bottom edge completely fixed in both the translational and rotational axis. However, just as the previous validation models suffered from this constraint, the models of the two panels also exhibited signs of inappropriate boundary condition choice. The plots of these models are included in Appendix E for comparison with the final model.

These earlier models show "fingers" of stress coming up from the fixed end of the panel and extending up to the second bead.

Upon inspection of the panel it was decided that only the corners of the bottom edge of the panel should be fixed. Thus the four extreme nodes on each side of the baseline were fixed both translationally and rotationally and the model rerun. This allowed the middle of the base line to deform into the z plane.

Once the new model had been run PAFEC's graphics tool, PIGS, was used to inspect the general results. Colour plots were generated for two stress types, these being Von Mises and stress in the y direction σ_{yy}. Both of these stress types were plotted for the inner and outer surfaces giving a total of four plots for each panel. These plots form Appendix F.

As can be seen from these plots, the effect of each of the beads is to cause the stress field to bend down and around the ends of the beads themselves. The plots also indicate that the beads themselves have a decreased stress field along their ridges. In this respect they are acting in a similar way to holes in a plate and thus the beads are acting as stress concentrators.

This "hole effect" has also been found in other beaded panels such as indicated in the reports into the collapse of the wing leading edges of an Orion P-3C (Ref. 2, 3). These reports concluded that the presence of dimples, designed to increase the shear stiffness of the rib, acted like holes in the structure. Their presence created a stress concentration factor of approximately 3.

As the curvature increases up the panel, bands of stress can be seen extending horizontally across the panel as would be expected because, as shown earlier, stress is directly proportional to curvature. However as the beads cause a reduced stress field they act to increase the stress surrounding them particularly at each end where the stress field bends down.

These results correspond to the actual failure sites on Australian Army aircraft. Each of the cracks that have been found have occurred at the end of the beads running at approximately 45° from the panel axis and in the same areas where the plots show a higher stress area.

Due to the nature of the panel's curvature, the inner surface is placed in compression, the outer surface in tension, and the absolute stress increases up the panel. The compression on the top surface could reasonably be expected to reduce the likelihood of crack growth high on the panel (where the compressive stress is greatest). However the tension on the back surface of the panel will tend to increase the likelihood of crack

growth. Thus cracks will tend to start on the back surface of the panel (and be harder to see).

Unfortunately due to the modelling process there still exists a slight end effect due to the choice of boundary conditions. In the following discussion, selection of stresses will be confined to the middle three beads and their immediate surrounds.

The stress results in terms of Von Mises stress concentrations are shown in Tables 4a and 4b. The plots in Appendix F give adequate indications of the stress field for both Von Mises stress and stress in the y direction (that is a vertical stress) on the panel. The aft edge of the panel is the side of the panel with the doubler. The forward edge has no doubler.

Panel 1 and Panel 2 almost overlap except for one bead with Panel 1 running from WL 257.000 to WL 242.944 and Panel 2 running from WL 252.245 to WL 238.606. However the top bead, and the half-bead at the bottom, are ignored because of end effects. For the purpose of discussion, the panel beads will be numbered as shown in Fig. 6 .

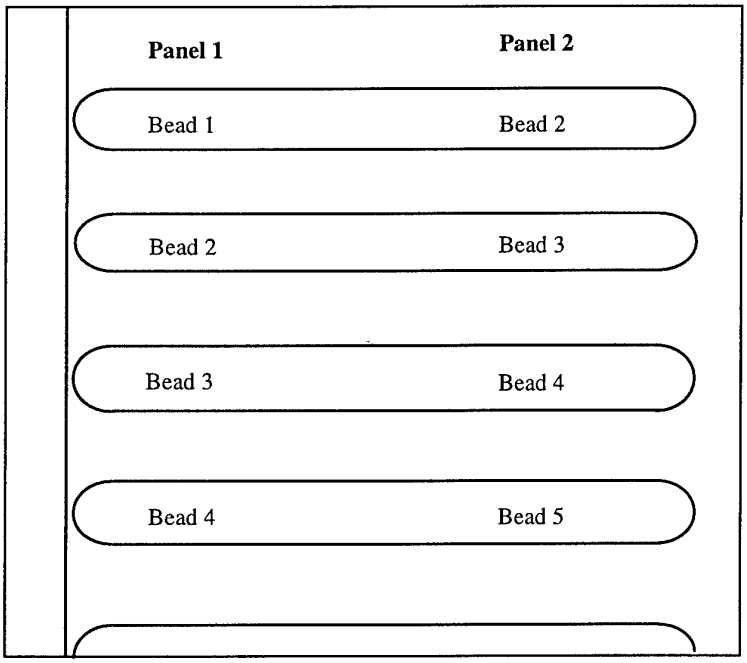

Figure 6. Naming Convention of Beads.

Table 4 (a). Forward edge of the panel.

Bead No.	Position[a]	Panel 1 Panel Stress[b] (MPa)	Panel 1 Flat Panel Stress[c] (MPa)	Panel 1 Stress Conc.[d]	Panel 2 Panel Stress (MPa)	Panel 2 Flat Panel Stress (MPa)	Panel 2 Stress Conc.
2	Top	115	85.0	1.4	-	-	-
	Bottom	117	74.5	1.6	-	-	-
3	Top	79.1	55.0	1.4	73.9	53.1	1.4
	Bottom	83.2	50.1	1.7	74.4	47.2	1.6
4	Top	56.1	39.2	1.4	52.4	35.0	1.5
	Bottom	68.4	36.7	1.9	53.3	35.8	1.5
5	Top	-	-	-	54.0	38.7	1.4
	Bottom	-	-	-	67.4	32.8	2.1

Table 4 (b). Aft edge of the panel.

Bead No.	Position	Panel 1 Panel Stress (MPa)	Panel 1 Flat Panel Stress (MPa)	Panel 1 Stress Conc.	Panel 2 Panel Stress (MPa)	Panel 2 Flat Panel Stress (MPa)	Panel 2 Stress Conc.
2	Top	135.7	86.1	1.6	-	-	-
	Bottom	138.1	75.3	1.8	-	-	-
3	Top	94.2	54.7	1.7	87.2	55.4	1.6
	Bottom	97.1	50.3	1.9	88.5	48.2	1.8
4	Top	67.2	39.3	1.7	62.2	35.6	1.8
	Bottom	77.0	37.4	2.1	62.5	34.6	1.8
5	Top	-	-	-	65.3	40.4	1.6
	Bottom	-	-	-	75.8	33.5	2.3

(a) Position - This is where the stress values have been obtained from. Fig. 2 indicates that "Top" means the top side of the bead and "Bottom" means the bottom side of the bead.

(b) Panel Stress - This is the maximum stress from the beaded panel model along the Top or Bottom as appropriate.

(c) Flat Panel Stress - This is the maximum stress, at the same location as the corresponding bead, from a dimensionally similar panel but without the beads, that is a flat panel, but using the same prescribed displacements.

(d) Stress Concentration - This is calculated by dividing the Panel Stress by the Flat Panel Stress.

As Table 4 shows, in general, the bottom of a bead experiences a higher stress concentration than the top of the bead. This is because the presence of the bead acts to increase the local curvature of the panel at the bottom of the bead more than at the top. This in turn generates a higher stress and stress concentration.

Also the aft edge of the panel shows higher stress concentrations than the forward edge of the panel. This is probably due to the presence of the doubler on the aft edge of the panel. The sharp edge of the doubler will locally increase the panel stress caused by any out-of-plane movement in the panel.

Table 1 of Ref. 4 shows the position of cracks in the Black Hawk fleet as at 5th August 1994 and this indicates that all of the cracks are on the upper side of the aft edge or the lower side of the forward edge. In addition 12 of the 64 cracks are on bead number 5 which the preceding results indicate is the bead with the highest stress concentration.

The positioning of the cracks diagonally opposite each other would seem to indicate shearing of the panel as a major contributor to the cracking. The effect of the superposition of the shearing action and the installation-induced stress is most extreme on the upper side of the aft edge of the panel and the lower side of the forward edge of the panel, where the cracks are occurring.

The plots of the results in Appendix F show that the bead itself is under almost no stress and is thus acting like a hole in the panel and therefore a stress concentrator.

3. CONCLUSION

Some S-70A-9 Black Hawk helicopters of the Australian Army are experiencing cracking on a starboard side internal fuselage skin panel which is riveted to fuselage frames FS295 and FS308.

Frames FS295 and FS308 are curved and the panel is brought into its final position by hand pressure. The aircraft drawings do not indicate that any stress-relieving process is applied to the panel after installation. Thus forcing the panel into the correct shape will cause installation-induced stresses in it.

An FE analysis was conducted to obtain the panel installation-induced stress. The use of the FE analysis method was validated.

To keep the model to a workable size, only a portion of the panel was modelled. To ensure that this model was producing reasonable results, a second model was made which partially overlapped the first.

The beads in the panel are subject to a much lower stress along each bead ridge and thus act like a hole in the panel and give rise to a significant stress concentration. This stress concentration is particularly obvious at each end on the upper and lower sides of each bead.

Numerically the stress concentrations range from 1.4 to 2.1 on the forward edge of the panel and from 1.6 to 2.3 on the aft edge of the panel. Also importantly the maximum stress is 140 MPa which occurs on the bottom side of the second bead from the top on the aft edge of the panel. As the yield strength of the aluminium alloy is in the region of 300 MPa, this represents a significant percentage of yield. It is worth emphasising that this is the installation-induced stress from the panel installation process.

The results obtained indicate a maximum stress concentration occurs on the fifth bead from the top on the aft edge of the panel and this correlates well with known crack locations on in-service Black Hawks.

The installation-induced stress is only one part of the stress applied to the panel. The panel is undergoing a complex loading pattern consisting of a variety of vibratory loads as well as significant loads from the side force and lift of the tail rotor. The panel is also mounted on the two forward lift frames and these alone exhibit a complex loading pattern.

4. ACKNOWLEDGMENTS

The author would like to thank the many AMRL staff who contributed to the preparation of this report. In particular the following contributions are gratefully acknowledged:

- Mr Julian Paul for guidance and assistance in the preparation and interpretation of the Finite Element model.
- Mr Daryl Keeley for assistance with the running of the Finite Element and associated software packages.
- Mr Domenico Lombardo for assistance with the preparation of the model and the supply of relevant Sikorsky drawings.
- Mr Richard Callinan for assistance with editing and vetting the report.

5. REFERENCES

1 The PAFEC Users Manual, Version 8.1

2 Molent, L. *Structural Investigations Into the Collapse of the Wing Leading Edges of Orion P-3C,* Proceedings of the PICAST 2 - AAC 6 Conference, Melbourne, Australia, 20 - 23 March 1995, pp. 787 - 794.

3 Wong, A.K., Ryall, T.G. and Richmond, M.J.*Structural Assessment of the Orion P3 Wing Leading Edge Using a State-of-the-Art Thermal Imaging System,* Proceedings of the PICAST 2 - AAC 6 Conference, Melbourne, Australia, 20 - 23 March 1995, pp. 795 - 800.

4 Lombardo, D.C., Patterson, A.K., Ferrarotto, P., Dutton, S.A., Powlesland, I.G. and Fraser, K.F.*Preparation of S-70A-9 Black Hawk Helicopter for Flight Tests to Investigate Cause of Cracking of Inner Fuselage Panel,*DSTO Technical Note, DSTO-TN-0004, AR-009-205, February 1995.

5 Higdon, A., Ohlsen, E., Stiles, W., Weese, J. and Riley, W. *Mechanics of Materials 4th Edition,* Brisbane, John Wiley and Sons, 1985, p360.

Appendix A
Element Validation

A1. Element Validation

To model the fuselage panel using an FE analysis, an element type needs to be chosen. Due to the nature of the panel (a relatively thin section) a plate element was selected. To validate the results produced by the plate element, a simple test case was examined. The test case was such that it could be solved analytically using existing conventional plate bending theory.

The test item is a standard cantilevered beam of length 200 mm, width 20 mm and thickness 1.27 mm, the same thickness as the actual panel. The beam is completely restrained at one end and a point load of 10 newtons is applied at the midpoint of the other end as shown in Fig. A1.

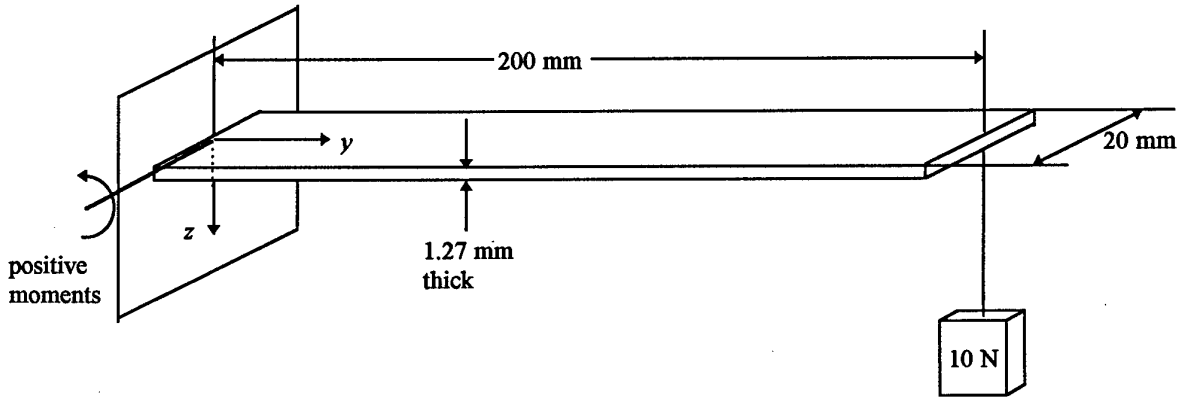

Figure A1. Simple Cantilevered Beam for Element Test

A2. Analytical Result.

The analytical method chosen to find deflections of the beam is the Method of Integration and the stresses in the beam are found using the Elastic Flexure Formula. The theory for the analytical solution is taken from Reference 1 and the derivation is contained in Appendix B.

The assumptions made in the derivation are:

- The resulting deflection is small compared to the length of the beam.
- The beam deflection due to shearing stresses is negligible (ie. a plane section is assumed to remain plane).
- The values of Young's Modulus (E) and the Moment of Inertia (I) remain constant, or are able to be expressed as a function, along the beam.
- The stresses remain within the elastic limit.

- The following sign convention, working from the left hand end, is utilised: Y is positive to the RIGHT, Z is positive DOWN and a POSITIVE MOMENT is COUNTER-CLOCKWISE (Fig. A1).

From Appendix B the deflection, z, at any point, y, along the beam is given by the equation:

$$z = \frac{1}{EI}\left(\frac{PL}{2}y^2 - \frac{P}{6}y^3\right)$$

To calculate the stress in the beam the Elastic Flexure Formula will be used and this is normally written as follows (Ref .1):

$$\sigma = -\frac{M.z_n}{I}$$

where σ is the flexural stress induced by a moment, M, at a distance, z_n , from the neutral axis of a beam with Moment of Inertia, I.

For the analytical result the above equations will be evaluated using the following values from Fig. A1.

$P = 10$ N

$L = 200$ mm

$E = 70\,000$ MPa (for aluminium)

In addition the maximum stress is calculated based on the maximum distance from the neutral axis, z_n. As the beam has a rectangular section the maximum distance is equal to the thickness of the beam (1.27 mm) divided by 2. Thus $z_n = 0.635$ mm.

The remaining constant to be found is the second moment of area, I. This is calculated using (Ref. 5):

$$I = \frac{bd^3}{12}$$

with b = width = 20 mm, and d = thickness = 1.27 mm.

Thus $I = 3.414$ mm^4

This will give moments in N.mm and stresses in MPa.

Elementary substitution of the above values into the equations for Moment, Deflection and Stress at the root ($y = 0$ mm), midpoint ($y = 100$ mm) and end ($y = 200$ mm) of the beam provides the results summarised in Table A1.

Table A1. Summary of analytical validation results.

y (mm)	Moment (N.mm)	Deflection (mm)	Stress (MPa)
0	-2000	0	372
100	-1000	34.9	186
200	0	111.6	0

A3. Finite Element Results.

After an analytical solution to the cantilevered beam test problem had been found a finite element model of the same problem was constructed. This problem is a rudimentary one for the finite element method so an answer of high accuracy was expected.

The model constructed is shown in Fig. A2 and indicates that the element mesh is 4 elements wide and 40 elements long. When associating this mesh with the actual problem each element becomes 5 mm in length and width.

The panel has a small thickness-to-length ratio. In such situations, the PAFEC User's Manual (Ref. 1) recommends that element type "44210 and other thin elements" would be the most appropriate. However, although appropriate for this problem, the element would not be appropriate for modelling the actual Black Hawk panel. Element type 44210 can only be used in situations where flatness is preserved, but this condition cannot be met on the actual panel because of its complex curvature. Hence, element type 43210 was selected as being more appropriate. This is also an eight noded shell element but without the restriction on preserving flatness. However, shear is not catered for by this element and thus the shells need to be thin.

To simulate the cantilevered problem one end of the model is completely fixed. In PAFEC this corresponds to a restraint module of 123456. 123 refers to translational motions in each of the primary axis (x, y, z respectively) and 456 refers to the rotational motions about the same axis set.

A point load of 10 newtons is placed on the opposite end of the model. As this is a rudimentary model a point load is sufficient. A higher accuracy (particularly at the loaded end) would be found by distributing the load more evenly across the end line of nodes.

Two problems arise out of this approach. Both are due to the limitation in the analytical theory as it ignores Poisson's strain.

When the beam is cantilevered, and force applied as shown in Fig. A2, the bottom surface is placed in compression and the top surface is placed in tension. Poisson's

strain predicts that to maintain volumetric continuity the top surface will shrink laterally and the bottom surface will expand laterally (that is across the x-axis). This causes the panel to warp around the y-axis instead of remaining straight.

Thus at the root, where all motion has been restrained, the stress field will exhibit fluctuations. As the analytical theory does not take this shrinkage into account the value it predicts at points around the root of the beam will be completely different to the values predicted by the finite element model (and in reality). Fortunately this effect is only apparent at the very base of the cantilevered beam. However, this means that the FE model results at the root cannot be compared directly with the analytical solution. The FE model results for nodes near the root will need to be extrapolated to the root to provide stresses which should be comparable to those predicted by the analytical method.

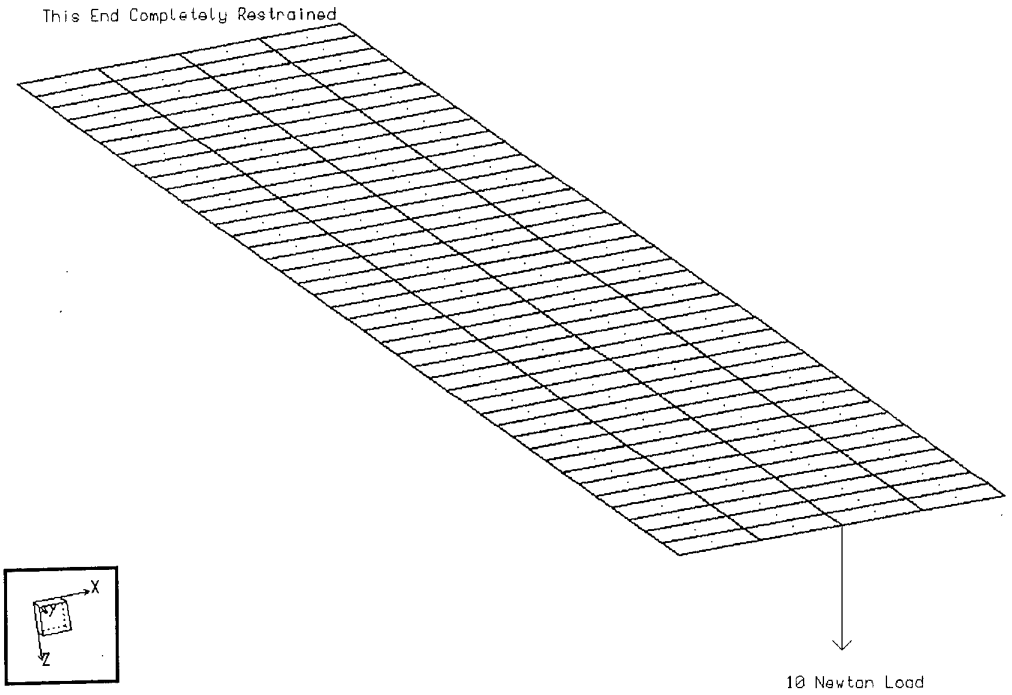

Figure A2. Mesh, Load and Restraint of the Element Test Model

The second problem occurs at the loaded end. At this point the distortion due to Poisson's shrinkage is at a maximum. Thus the displacement predicted by the FE model at an edge node will be slightly less than at a more central node as can be seen in the exaggerated view of Fig. A3. As the analytical method does not take this into account its prediction of displacement at this end will be uniform across the end. However, the results should still be quite close and the *average* of FE model displacements across the beam will be used to compare results.

The FE model predictions of the stress field at the root and the displacement field at the tip are closer to reality, but there is no easy analytical approach to check this.

Inspection of the PAFEC output file (extension .O02) yields the node numbers corresponding to y = 0 mm, y = 100 mm and y = 200 mm which are the points chosen to compare the analytical solution with the computational (FE) result. These are outlined in Table A2.

Table A2. Nodal information for comparison points.

y (mm)	Nodes
0	1, 2, 5, 6, 7, 8, 9, 10, 11
100	283, 284, 285, 286, 287, 288, 289, 290, 291
200	3, 4, 563, 564, 565, 566, 567, 568, 569

Inspection of the PAFEC displacement output file (extension .O07) yields the displacement at each node in the model. Displacements for the node numbers corresponding to y = 0 mm, y = 100 mm and y = 200 mm were extracted from this file and these are outlined in Table A3.

Table A3. Displacement of selected nodes.

y mm	Node	Displacement mm	y mm	Node	Displacement mm	y mm	Node	Displacement mm
0	1	0	100	283	34.283	200	3	110.443
0	2	0	100	284	34.310	200	4	110.443
0	5	0	100	285	34.330	200	563	110.447
0	6	0	100	286	34.342	200	564	110.451
0	7	0	100	287	34.346	200	565	110.454
0	8	0	100	288	34.342	200	566	110.456
0	9	0	100	289	34.330	200	567	110.454
0	10	0	100	290	34.310	200	568	110.451
0	11	0	100	291	34.283	200	569	110.447
Average			100		34.32	200		110.45

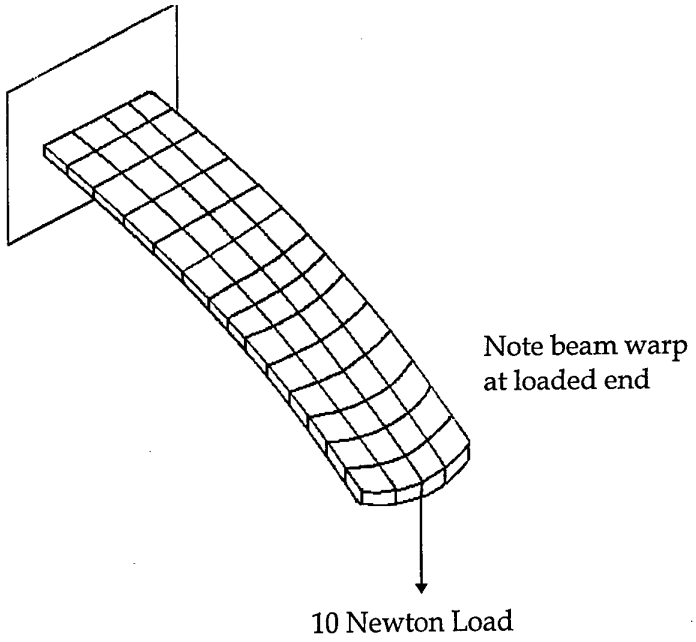

Figure A3. View of Distorted End Displacements (exaggerated).

Inspection of the PAFEC stress output file (extension .O09) yields the principal stresses at each node in the model. These were added (using vector addition) to give the fibre stresses at the node numbers corresponding to y = 100 mm. These stresses together with their average are given in Table A4.

Table A4. Stress at the nodes with position y = *100 mm.*

Node	Stress (MPa)
283	186.00
284	186.00
285	186.00
286	186.00
287	186.00
288	186.00
289	186.00
290	186.00
291	186.00
Average	**186.00**

Due to the limits of the analytical theory, as outlined earlier, the stress at $y = 0$ mm had to be extrapolated. A plot of stress versus distance along the beam is shown in Fig. A4. The value for Average Stress comes from an average of stresses at each section along the beam.

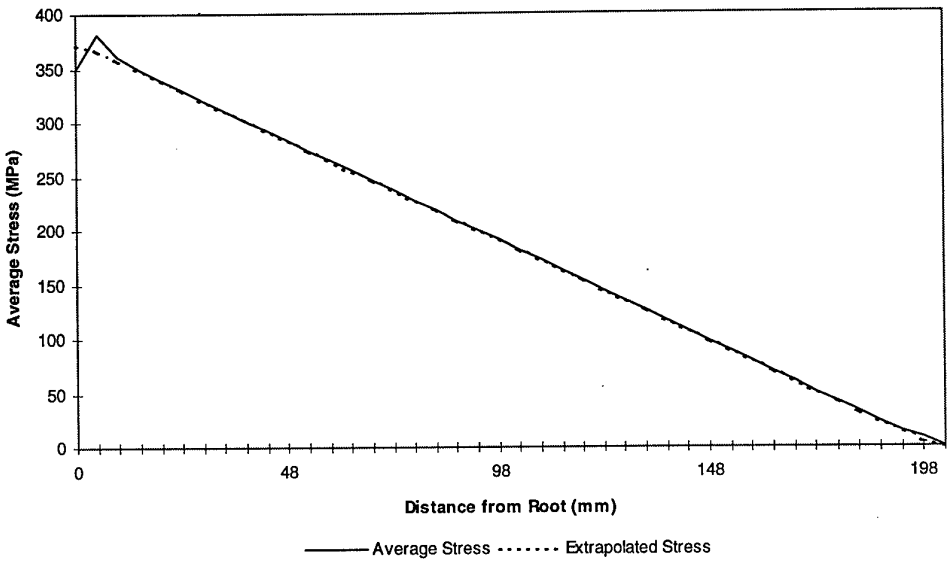

Figure A4. A Plot of Average Stress v. Distance Along the Beam From the Root.

When the extrapolated line is extended to the root ($y = 0$ mm) it is found to give a stress of **372 MPa**.

A4. Comparison: Analytical v. FE Model

The results of the two types of solution discussed in the previous sections are summarised in Table A5.

Table A5. Summary of analytical and FE model results.

y (mm)	Analytical Solution	FE Model Solution	Percentage Error*
0	372 MPa	372 MPa	0.0
100	186 MPa	186 MPa	0.0
100	34.9 mm	34.3 mm	-1.7
200	112 mm	111 mm	-1.0

* Error based on Analytical Solution.

Minor discrepancies were to be expected because the analytical approach ignored Poisson's Effect which causes the beam to deform around a longitudinal axis due to stretching of the bottom surface and shrinking of the top surface. This effect also acts at the root of the beam to cause an end effect.

However as can be seen from the summary table (Table A5) the discrepancies are minor (less than 1.7 % in all cases). The stress at the root was found with a simple extrapolation of results to the root. Thus the conclusion is that element type 43210 is suitable for this type of loading.

Appendix B
Derivation of Analytical Equations

B1. Derivation of Analytical Equations for Element Validation

In order to assess the validity of the plate element chosen to model the panel a comparison of a PAFEC generated solution with a manually calculated solution was conducted. The method chosen to find deflections of the beam is the Method of Integration and the stresses in the beam are found using the Elastic Flexure Formula. The theory for the manual solution is taken from Reference 1.

Note that the following limitations only apply to the analytical solution of the validation problem.

The assumptions are:

- The resulting deflection is small compared to the length of the beam.
- The beam deflections due to shearing stresses are negligible (ie. a plane section is assumed to remain plane).
- The value of Young's Modulus (E) and the Moment of Inertia (I) remain constant, or are able to be expressed as a function, along the beam.
- The stresses remain within the elastic limit.
- The following sign convention, working from the left hand end, is utilised: y is positive to the RIGHT, z is positive DOWN and a POSITIVE MOMENT is COUNTER-CLOCKWISE.

A freebody diagram of the problem in general terms is shown as Fig. B1. The details of the beam are as shown in Fig. A1.

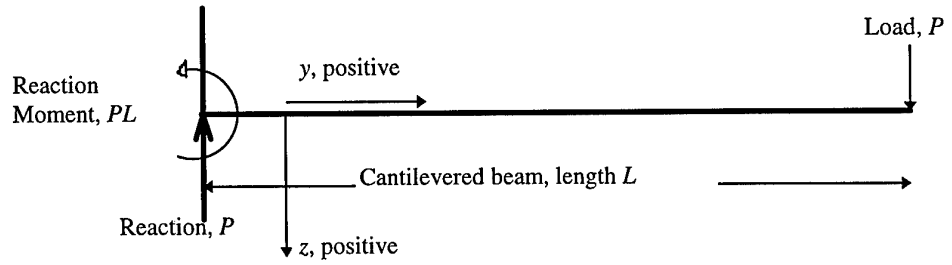

Figure B1. Freebody Diagram of Element Validation Problem .

The Method of Integration is based on the following equations.

$$deflection = -z$$

$$slope = \frac{dz}{dy}$$

$$moment = M = EI\frac{d^2z}{dy^2}$$

$$shear = \frac{dM}{dy} = EI\frac{d^3z}{dy^3}$$

By inspection of the freebody diagram, Fig. B1, and following the sign conventions outlined earlier, the shear force along the beam is constant at $+P$. Thus

$$shear = \frac{dM}{dy} = EI\frac{d^3z}{dy^3} = P$$

Upon integrating once to find the moment, with C_1 as the constant of integration, the following results:

$$M = Py + C_1$$

At $y = 0$, $M = -PL$ and thus $C_1 = -PL$. This is confirmed at $y = L$, $M = 0$.

$$M = Py - PL$$

As already noted

$$M = EI\frac{d^2z}{dy^2} = Py - PL$$

Integrating once again to find the slope yields the following result, with C_2 as the constant of integration:

$$slope = \frac{dz}{dy} = \frac{1}{EI}\left(\frac{P}{2}y^2 - PLy + C_2\right)$$

At $y = 0$, slope = 0 (as it is built into the wall) an thus $C_2 = 0$.

Integrating once more to find the deflection gives the following result, with C_3 as the constant of integration:

$$deflection = -z = \frac{-1}{EI}\left(\frac{P}{6}y^3 - \frac{PL}{2}y^2 + C_3\right)$$

At $y = 0$, deflection = 0 (as, again, it is built into the wall) and thus $C_3 = 0$.

Upon rearranging the deflection, z, at any point, y, along the beam is given by the equation:

$$z = \frac{1}{EI}\left(\frac{PL}{2}y^2 - \frac{P}{6}y^3\right)$$

Appendix C
Method Validation

C1. Method Validation

The finite element method is normally used to find stress and displacement fields when a given set of forces is applied. However in this situation the installation-induced stress field is caused by the panel being pushed into shape (ie. a displacement field). Information regarding the displacement field was found from the relevant aircraft drawings[2].

Therefore, the FE analysis will involve applying a set of known (ie. prescribed) displacements to the nodes of the panel FE model and then examining the resultant stresses. However, it is important to test that the prescribed-displacement method will yield suitable results when applied to this element type and this type of structure.

To determine the response of the plate element to the prescribed-displacement method, a simple validation test was performed using PAFEC. As with the element type validation, the problem was such that it can be solved analytically using existing conventional plate bending theory. The analytical result is then compared with the Finite Element result.

A standard beam of length 200 mm, width 20 mm and thickness 1.27 mm will be considered, as before. The beam is forced into a constant curvature that can be described analytically. In this particular case the beam was displaced to form an arc of a circle 1000 mm in radius as shown in Fig. C1.

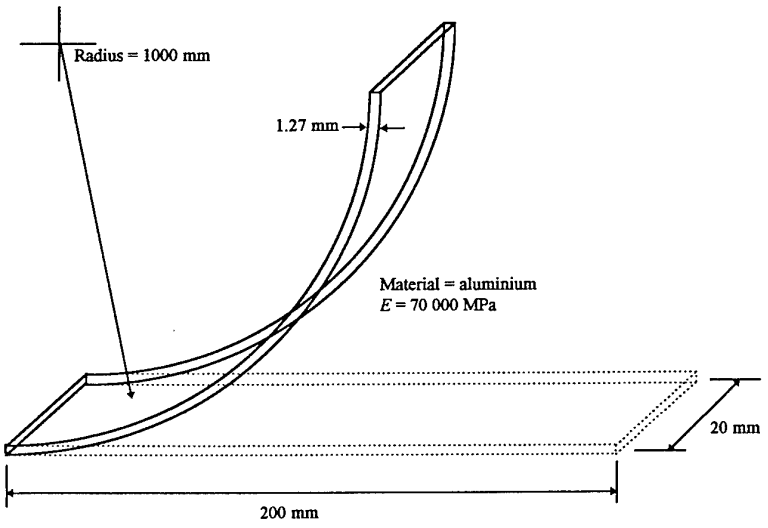

Figure C1. Curvature of Plate for Displacement Method Test.

[2] Sikorsky Drawing Number 70219 - 02130 Fitting Assy., Upper Fus. - STA308.00 (see Appendix B) with additional information from Sikorsky Drawing Number 70211 - 02107 Sht 1, Rev J Frame Instl., Upper Fus. - STA308.00

C2. Analytical Result

The method chosen to find the stresses in the beam was the Elastic Flexure Formula. The theory for the analytical solution is again taken from Reference 1.

The assumptions applicable to the analytical solution are:

- The beam deflection due to shearing stresses is negligible (ie. a plane section is assumed to remain plane).
- The value of Young's Modulus (E) and the Moment of Inertia (I) remain constant, or are able to be expressed as a function, along the beam.
- The stresses remain within the elastic limit.

The details of the beam are as shown in Fig. C1. A freebody diagram of a small section of the beam in general terms is shown in Fig. C2.

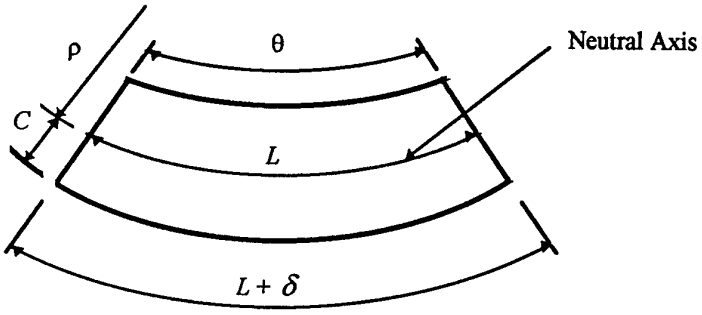

Figure C2. Freebody Diagram of Element Validation Problem.

When a straight beam is loaded within the elastic limit the neutral axis forms a curve called the elastic curve. In regions of constant bending moment, M, this curve is an arc of a circle of radius, ρ.

From Fig. C2:

$$L = \rho\theta$$
$$\text{and } L + \delta = (\rho + C)\theta$$

Hence:

$$\theta = \frac{L}{\rho} = \frac{L+\delta}{\rho+C}$$

which leads to:

$$\frac{C}{\rho} = \frac{\delta}{L}$$

where C is the distance from the neutral axis to the outer edge of the beam (in this case, C = half the beam thickness), and δ is the incremental increase in the length of the arc.

The right hand side of the final equation is the standard result giving strain. Thus

$$\frac{C}{\rho} = \frac{\delta}{L} = \varepsilon = \frac{\sigma}{E}$$

which gives:

$$\sigma = \frac{EC}{\rho}$$

where E is Young's Modulus.

This final equation thus relates the beam's thickness, $2C$, the radius of curvature, ρ and Young's Modulus, E, to the stress, σ, in the beam. If the beam has a constant radius of curvature, then it follows that the stress in the beam will be constant.

From Fig. C1, C = 1.27 / 2 = 0.635 mm, ρ = 1000 mm and E = 70 000 MPa. Hence, the stress in the panel is found to be:

$$\sigma = \frac{EC}{\rho} = \frac{70000 \times 0.635}{1000} = 44.5 \text{ MPa}$$

C3. Finite Element Results.

After an analytical solution to the constant radius of curvature beam test problem had been found a finite element model of the same problem was constructed. Again this problem is rudimentary and an answer of high accuracy (compared to the analytical solution) should be expected.

The model dimensions and other details such as element type are identical to those for the model used for the element validation problem which is shown in Fig. A2.

In order to simulate the problem one end of the model is translationally fixed. In PAFEC this corresponds to a restraint module of 123, which refers to translational motions in each primary axis (x, y, z respectively). However the model is allowed to rotate at the fixed end around these axes.

Initially the displacements of each node were calculated according to the equation:

$$z = 1000 - \sqrt{1000^2 - y^2}$$

and this displacement was applied to each node.

However it was found that this gave a resultant stress field that was higher than expected (typically 13%).

As a result of this the displacement field was not applied to each node but, rather, only to the nodes along each edge of the beam. This gave a better result as it allowed the model to curve (around the *y*-axis) according to Poisson's relationship as outlined in the element validation section (Appendix A). Again this model indicated a stress field higher than would be expected (typically 10%).

Finally, it was found that the initial equation was inaccurate as it was not taking into account the reduction in effective height as the panel curved to the arc shape. Here effective height is meant as the height above the *z*-axis datum. To account for this a different approach based on a circumferential equation was used. The derivation of this equation is shown with the aid of Fig. C3.

$$z = \rho - \rho\cos\theta$$

$$\therefore z = \rho\left(1 - \cos\left(\frac{y}{\rho}\right)\right)$$

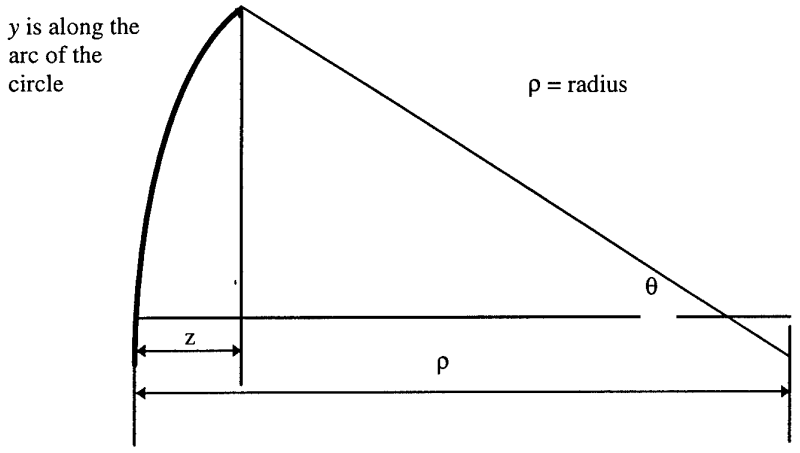

Figure C3. Derivation of Nodal Position Formula.

As explained in Appendix A.2 problems arise out of this approach due to the limitations of the analytical theory. The limitation is that the theory ignores Poisson's strain. However as the maximum deflection of the tip in the cantilevered beam case was of the order of 110 mm and in this case the displacement of the corresponding point is only some 20 mm the limitation of the theory should be expected to be much less. Indeed inspection of the results indicates that the panel is only warping some 0.006 mm across the 20 mm panel section.

At the root, where all translational motion has been restrained the stress field will exhibit fluctuations. As the analytical theory does not take shrinkage into account, the value it predicts at points around the root of the beam will be uniform and completely different to the values predicted by the finite element model (and in reality).

A problem also occurs at the tip of the beam. The analytical model does not take into account the shear stress. The effect of this is that the analytical result will be constant along the beam length whilst the FE model will predict a reduction in stress at both ends of the beam. The FE results for stress along the beam are shown in Table C1 and in Fig. C4.

The FE model predictions of the stress field at the root and at the tip are probably more accurate, but there is no easy analytical approach to check this.

Inspection of the stress file (extension .O09) yields the results shown in Table C1 for each of the 40 rows of elements along the beam. From Table C1, if the first and last 20 mm of the panel are ignored, then the maximum error is less than 3% and mostly less than 1%.

The reason that the percentage error increases along the beam, in areas outside the end effects, can be attributed to loss of numerical accuracy of the input equation that defines the initial displacement of the panel.

Overall, the conclusion is that the prescribed-displacement method, together with PAFEC element type 43210, are suitable for assessing the installation-induced stress in the Black Hawk panel.

Table C1. Tabulation of FE results for the method validation test.

Length Along Beam (mm)[a]	Edge Stress (MPa)[b]	Central Stress (MPa)[c]	Average Stress (MPa)[d]	Predicted Stress (MPa)[e]	% Error [f]
2.5	31.51	16.42	23.97	44.45	-46.08
7.5	40.13	33.59	36.86	44.45	-17.07
12.5	43.23	40.97	42.10	44.45	-5.28
17.5	44.11	43.57	43.84	44.45	-1.37
22.5	44.40	44.42	44.41	44.45	-0.08
27.5	44.50	44.51	44.50	44.45	0.12
32.5	44.50	44.50	44.50	44.45	0.12
37.5	44.50	44.50	44.50	44.45	0.11
42.5	44.40	44.50	44.45	44.45	0.00
47.5	44.40	44.40	44.40	44.45	-0.11
52.5	44.40	44.40	44.40	44.45	-0.11
57.5	44.40	44.40	44.40	44.45	-0.11
62.5	44.40	44.40	44.40	44.45	-0.11
67.5	44.30	44.40	44.35	44.45	-0.22
72.5	44.30	44.30	44.30	44.45	-0.34
77.5	44.30	44.30	44.30	44.45	-0.34
82.5	44.30	44.30	44.30	44.45	-0.34
87.5	44.30	44.30	44.30	44.45	-0.34
92.5	44.30	44.30	44.30	44.45	-0.34
97.5	44.20	44.20	44.20	44.45	-0.56
102.5	44.20	44.20	44.20	44.45	-0.56
107.5	44.20	44.20	44.20	44.45	-0.56
112.5	44.20	44.20	44.20	44.45	-0.56
117.5	44.10	44.10	44.10	44.45	-0.79
122.5	44.10	44.10	44.10	44.45	-0.79
127.5	44.10	44.10	44.10	44.45	-0.79
132.5	44.10	44.10	44.10	44.45	-0.79
137.5	44.00	44.00	44.00	44.45	-1.01
142.5	44.00	44.00	44.00	44.45	-1.01
147.5	44.00	44.00	44.00	44.45	-1.01
152.5	43.90	43.90	43.90	44.45	-1.24
157.5	43.90	43.90	43.90	44.45	-1.24
162.5	43.90	43.90	43.90	44.45	-1.24
167.5	43.80	43.90	43.85	44.45	-1.35
172.5	43.80	43.70	43.75	44.45	-1.57
177.5	43.60	43.41	43.50	44.45	-2.13
182.5	43.20	42.32	42.76	44.45	-3.80
187.5	42.11	39.32	40.72	44.45	-8.40
192.5	39.55	31.80	35.67	44.45	-19.74
197.5	35.49	16.59	26.04	44.45	-41.42

Length Along The Beam is the distance along the beam from the restrained end (0 mm) towards the free end (200 mm).

Edge Stress is the element stress in the first and fourth element of the row.

Central Stress is the stress in the second or third element of the row.

Average Stress is the average of (b) and (c).

Predicted Stress is the stress field from the analytical result.

% Error is the percentage difference between the predicted and the average stress based on the predicted stress.

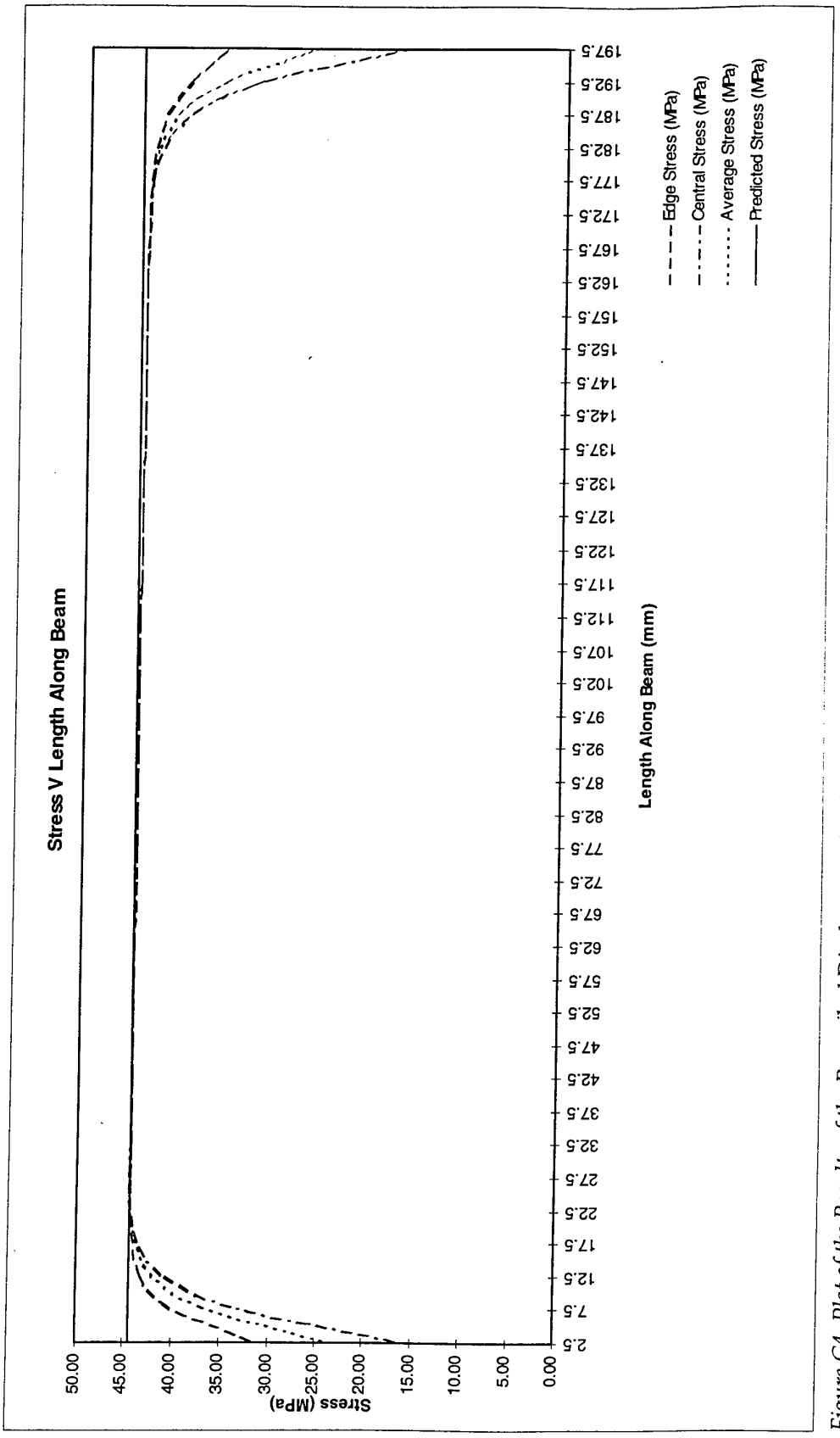

Figure C4. Plot of the Results of the Prescribed Displacement Method Validation Tests.

Appendix D
Extract From Sikorsky Drawing Number 70219 - 02130
Fitting Assy, Upper Fus - STA 308.00

X COORD	Z COORD

X COORD	Z COORD

CENTER CIRCLE "F"

18.000	29.485

CIRCLE "F"

13.002	38.147
9.340	34.486
8.000	29.485

COUNTOUR "E"

27.000	42.114
26.000	42.000
25.000	41.870
24.000	41.720
23.000	41.549
22.000	41.357
21.000	41.140
20.000	40.896
19.000	40.624
18.000	40.319
17.000	39.978
16.000	39.596
15.000	39.169
14.000	38.688
13.002	38.147

Extracted from Sikorsky Drawing:

DRAWING TITLE
FITTING ASSY, UPPER FUS - STA 308.00
DRAWING NUMBER
70219-02130

COORDINATES OF FITTING CONTOUR

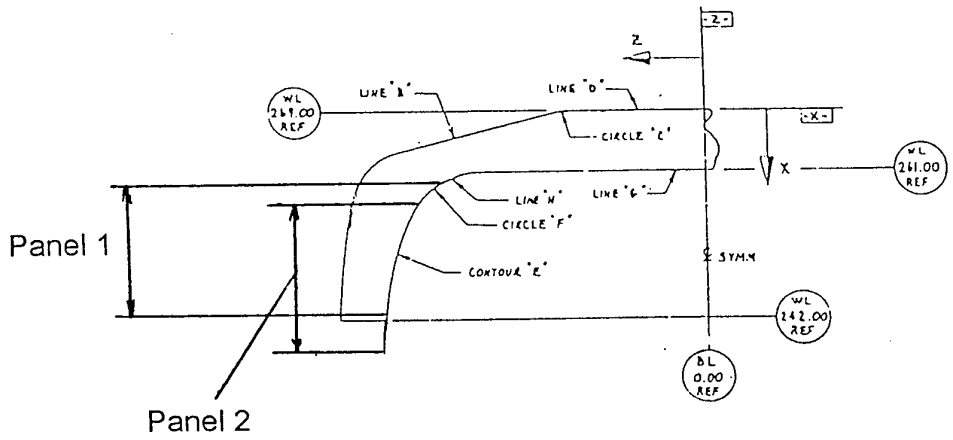

Appendix E
Plots of Fuselage Panel Stress Field with Bottom Edge Completely Fixed.

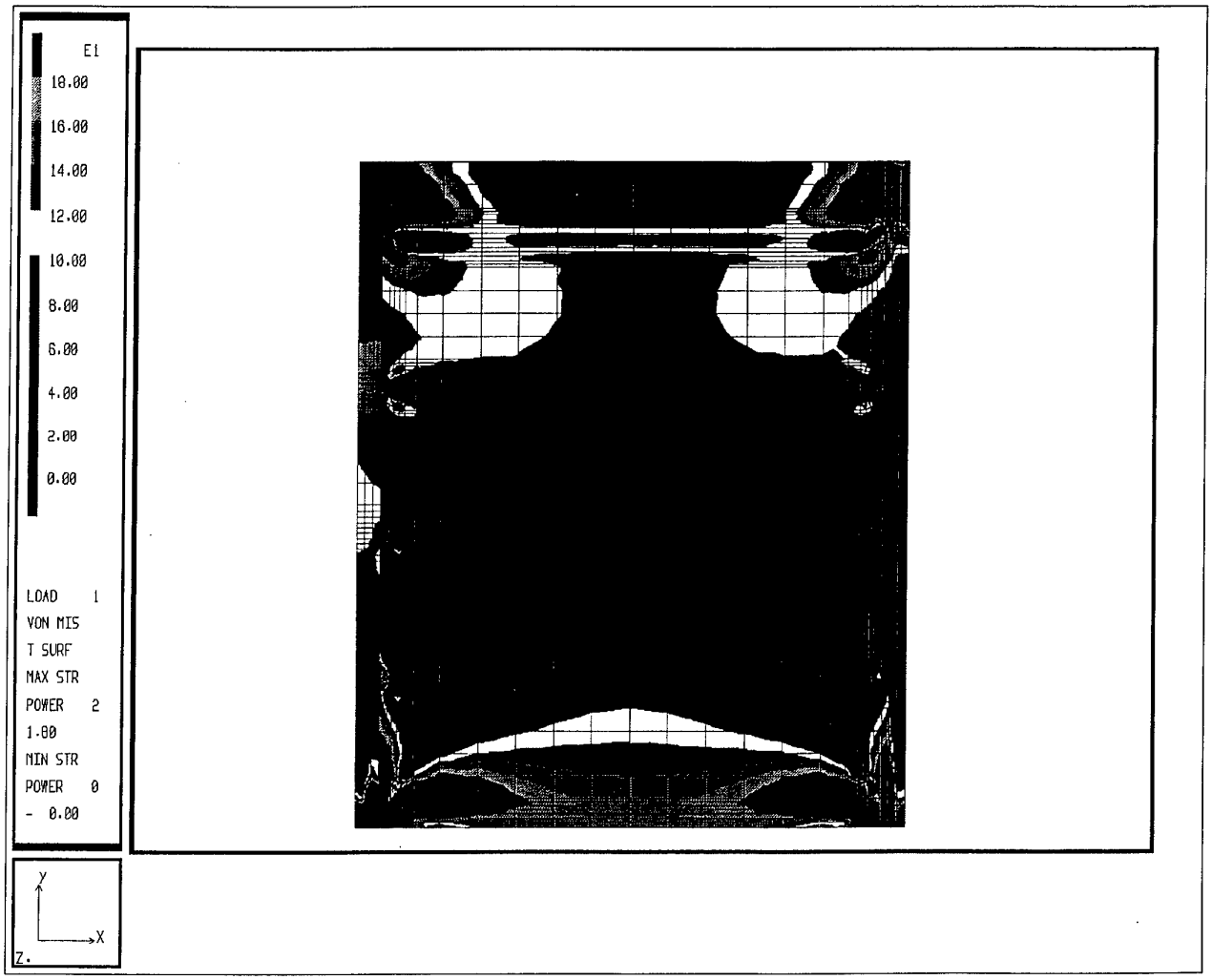

Figure E1. Von Mises Stress Field, Top Surface, Bottom Edge Fully Constrained

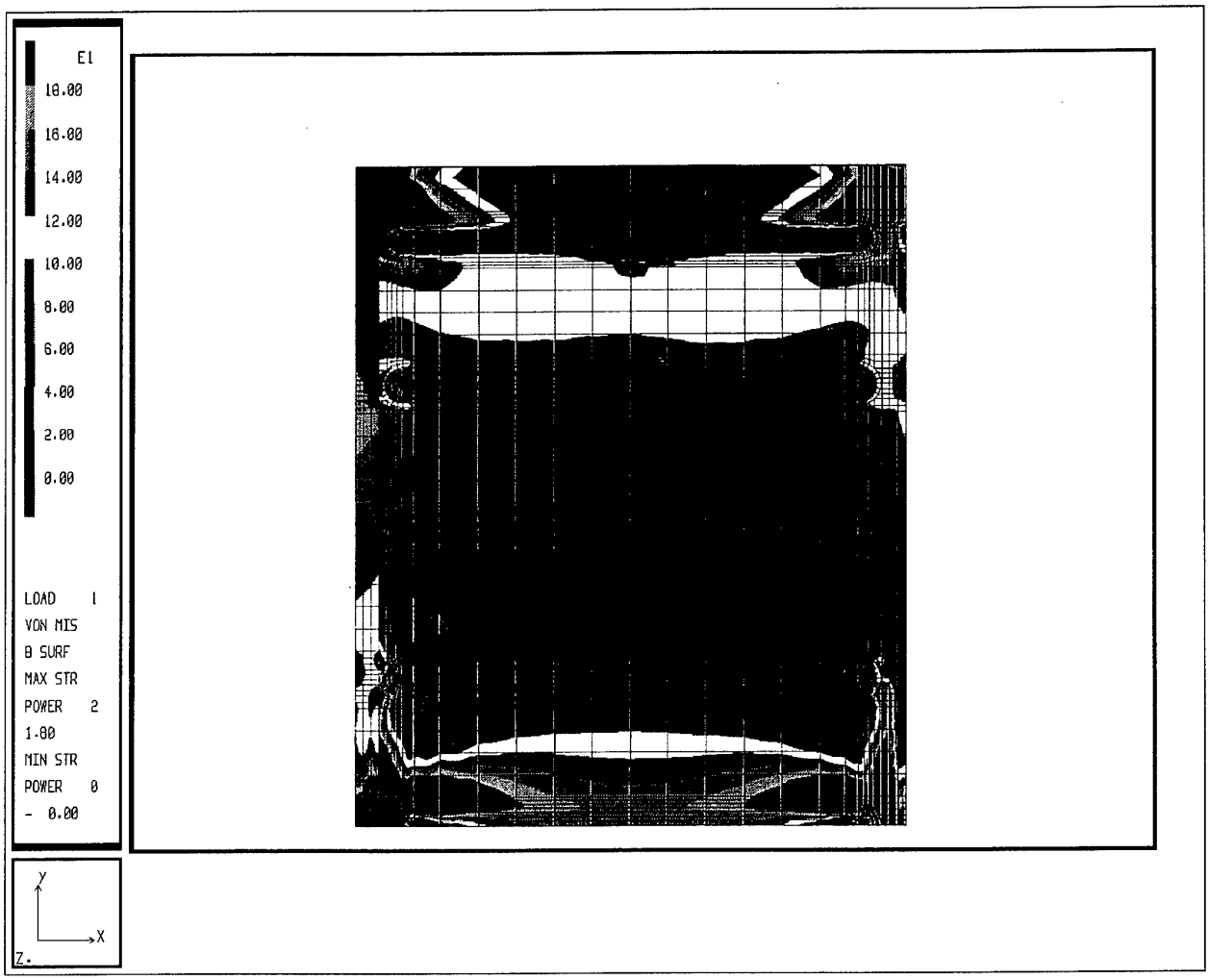

Figure E2. Von Mises Stress Field, Bottom Surface, Bottom Edge Fully Constrained

Appendix F
Plots of Fuselage Panel Stress Field with Bottom Edge Allowed to Translate Out of Plane

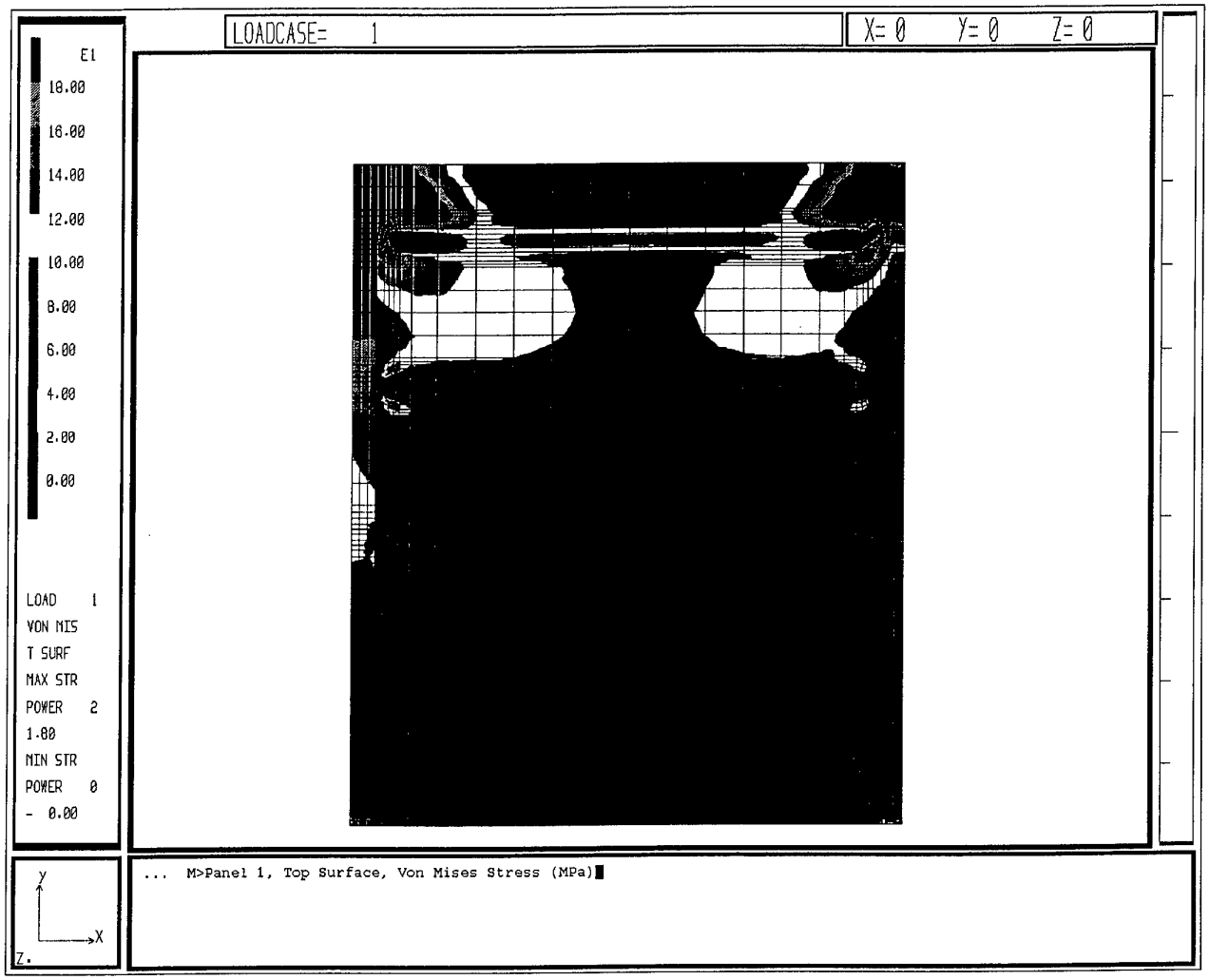

Figure F1. Panel 1 Top Surface Von Mises Stress.

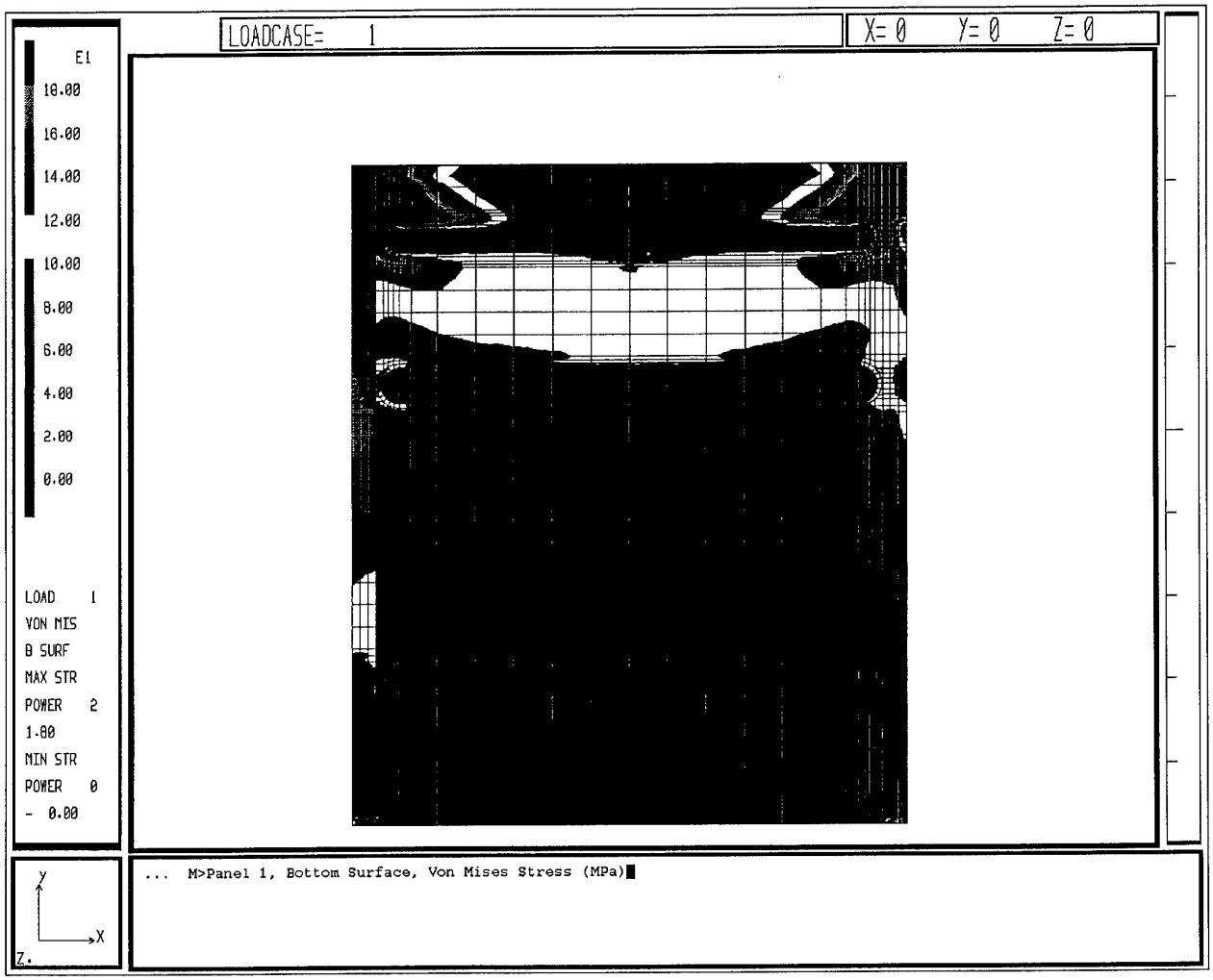

Figure F2. Panel 1 Bottom Surface Von Mises Stress

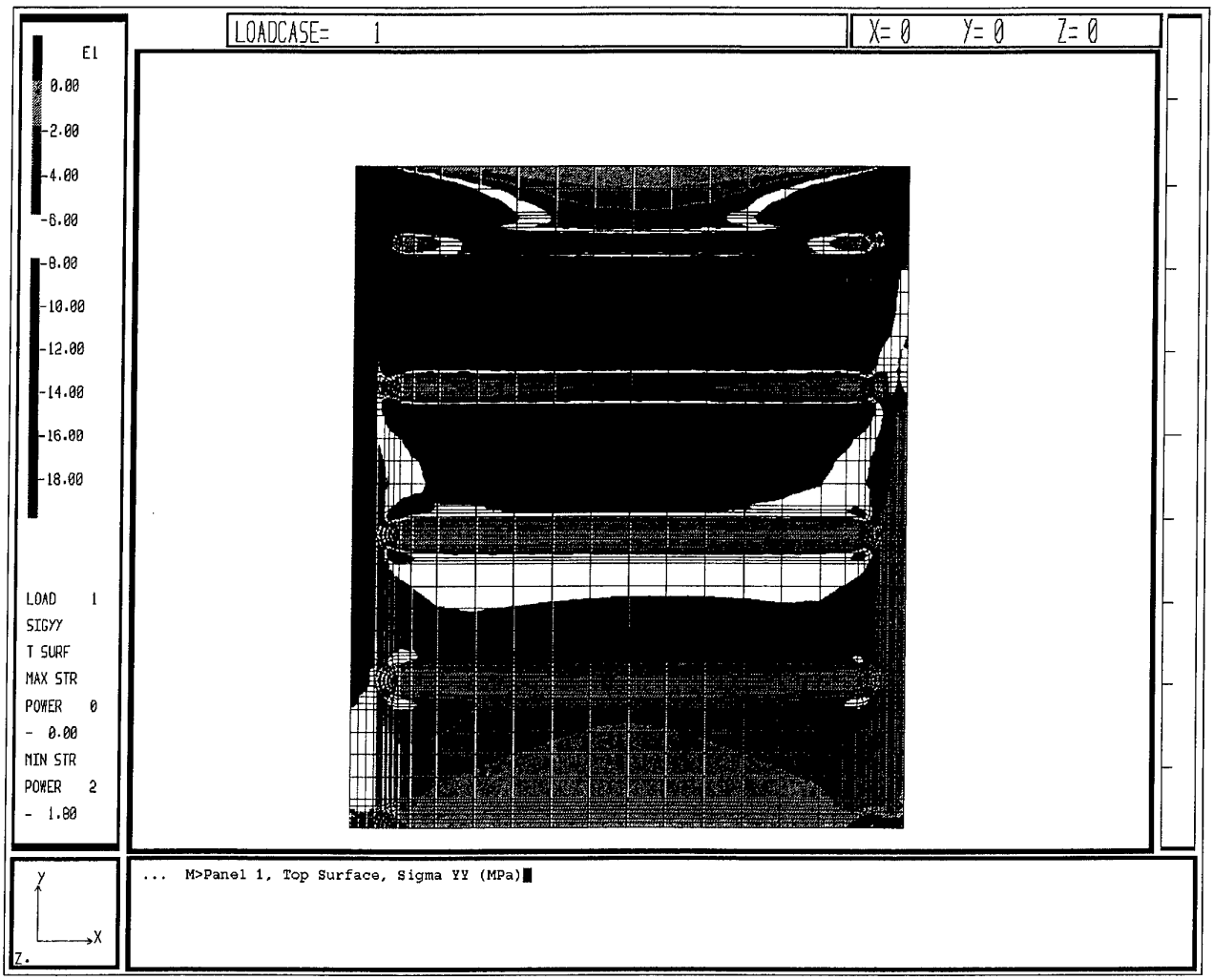

Figure F3. Panel 1 Top Surface sigma yy Stress

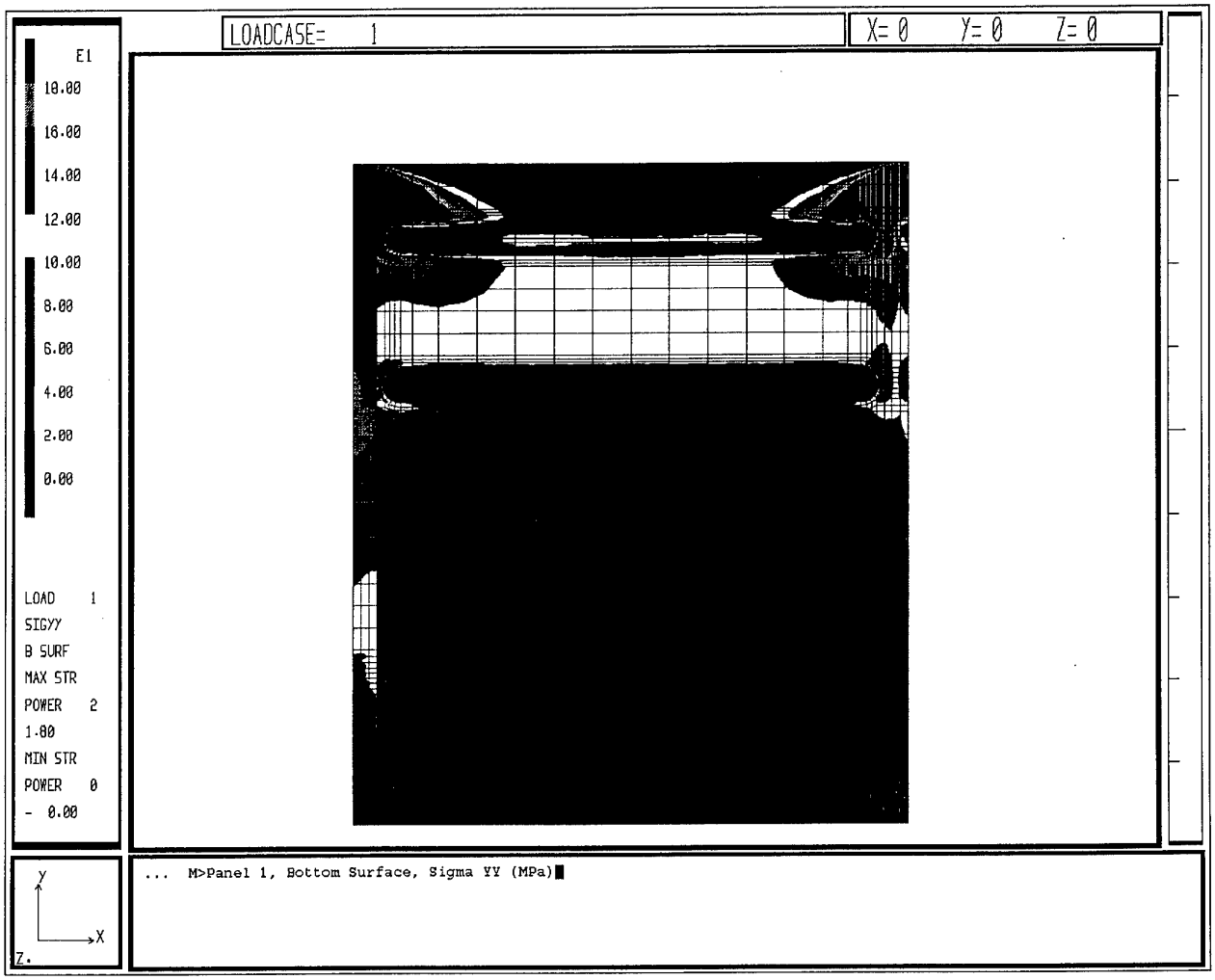

Figure F4. Panel 1 Bottom Surface sigma yy Stress

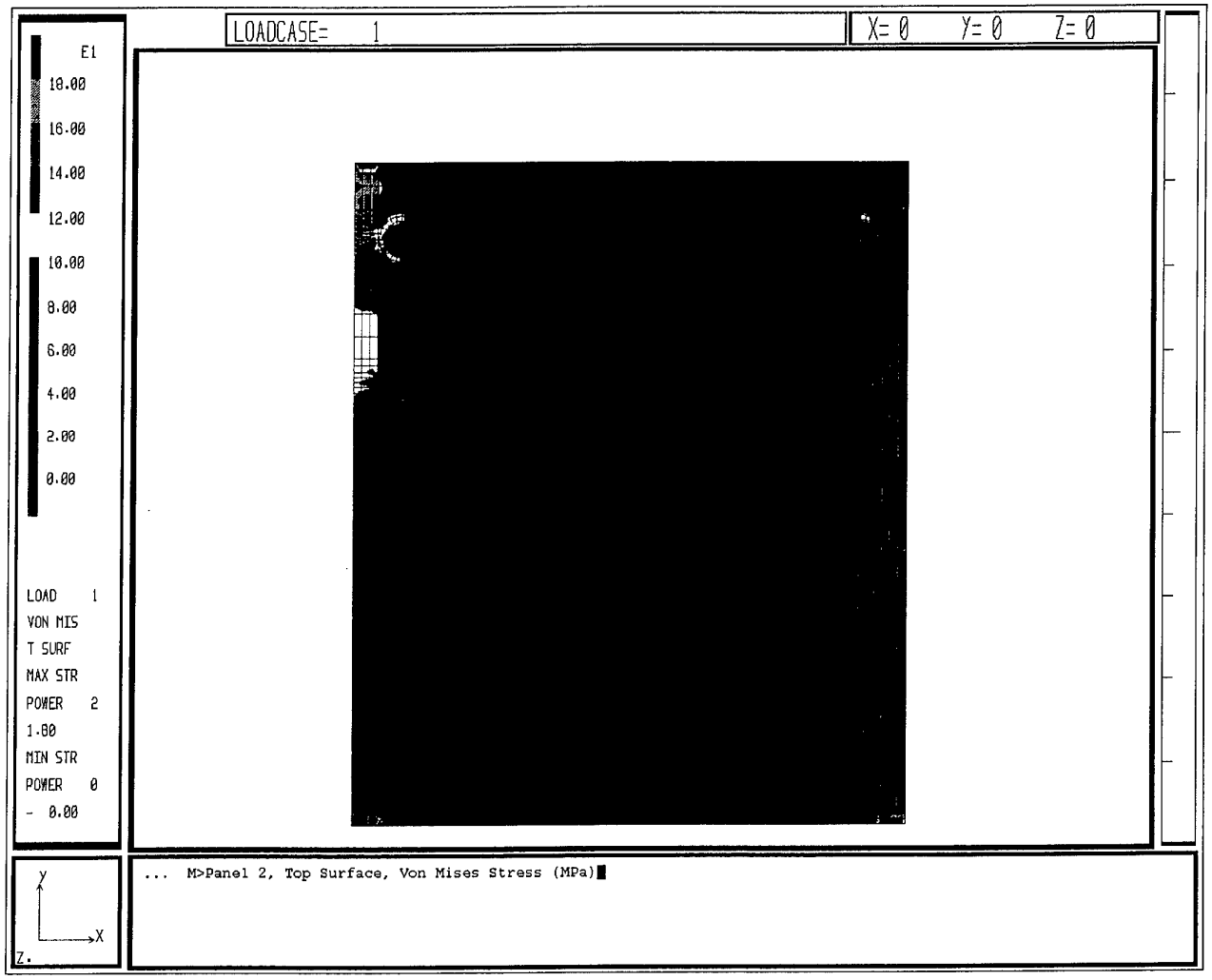

Figure F5. Panel 2 Top Surface Von Mises Stress

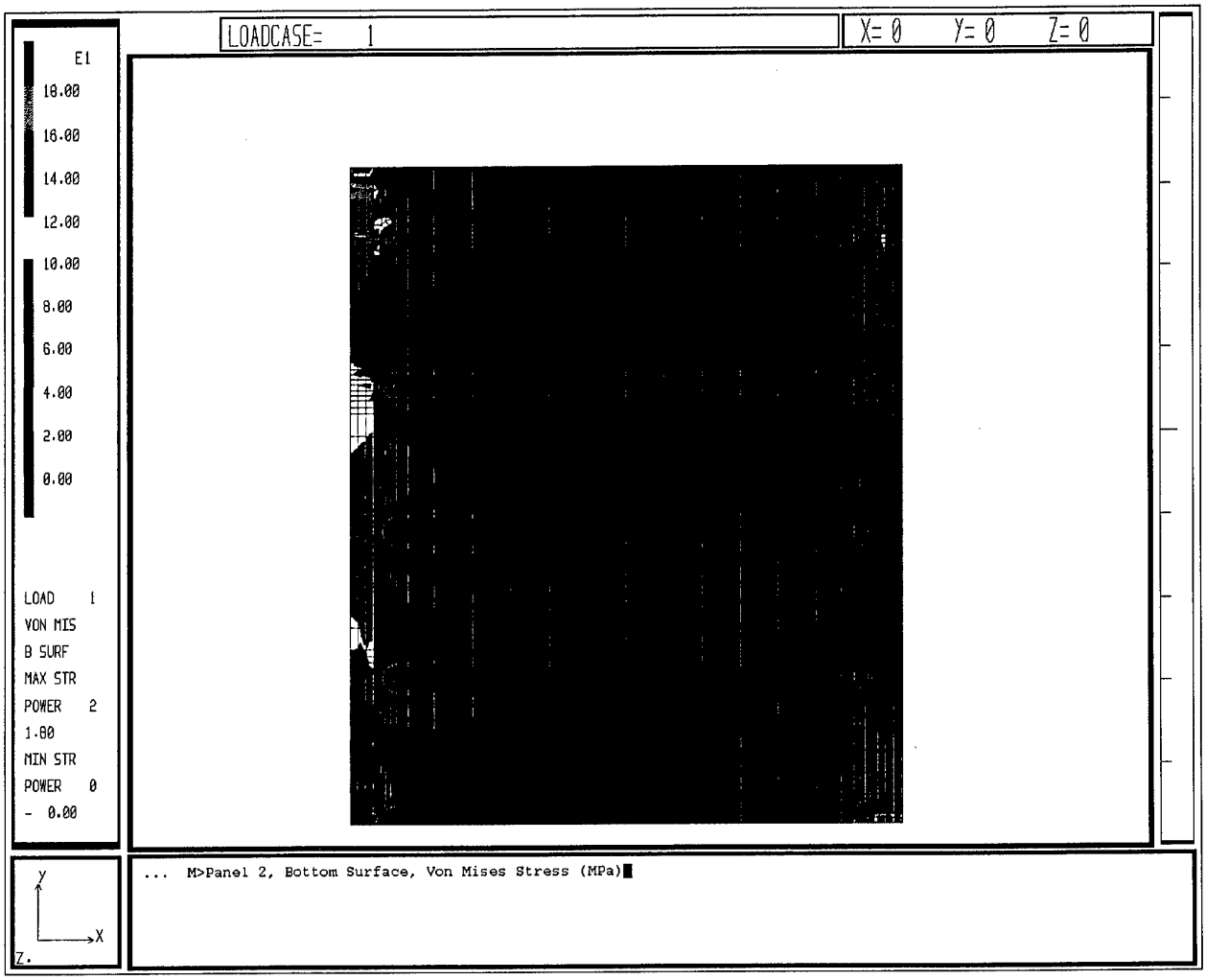

Figure F6. Panel 2 Bottom Surface Von Mises Stress

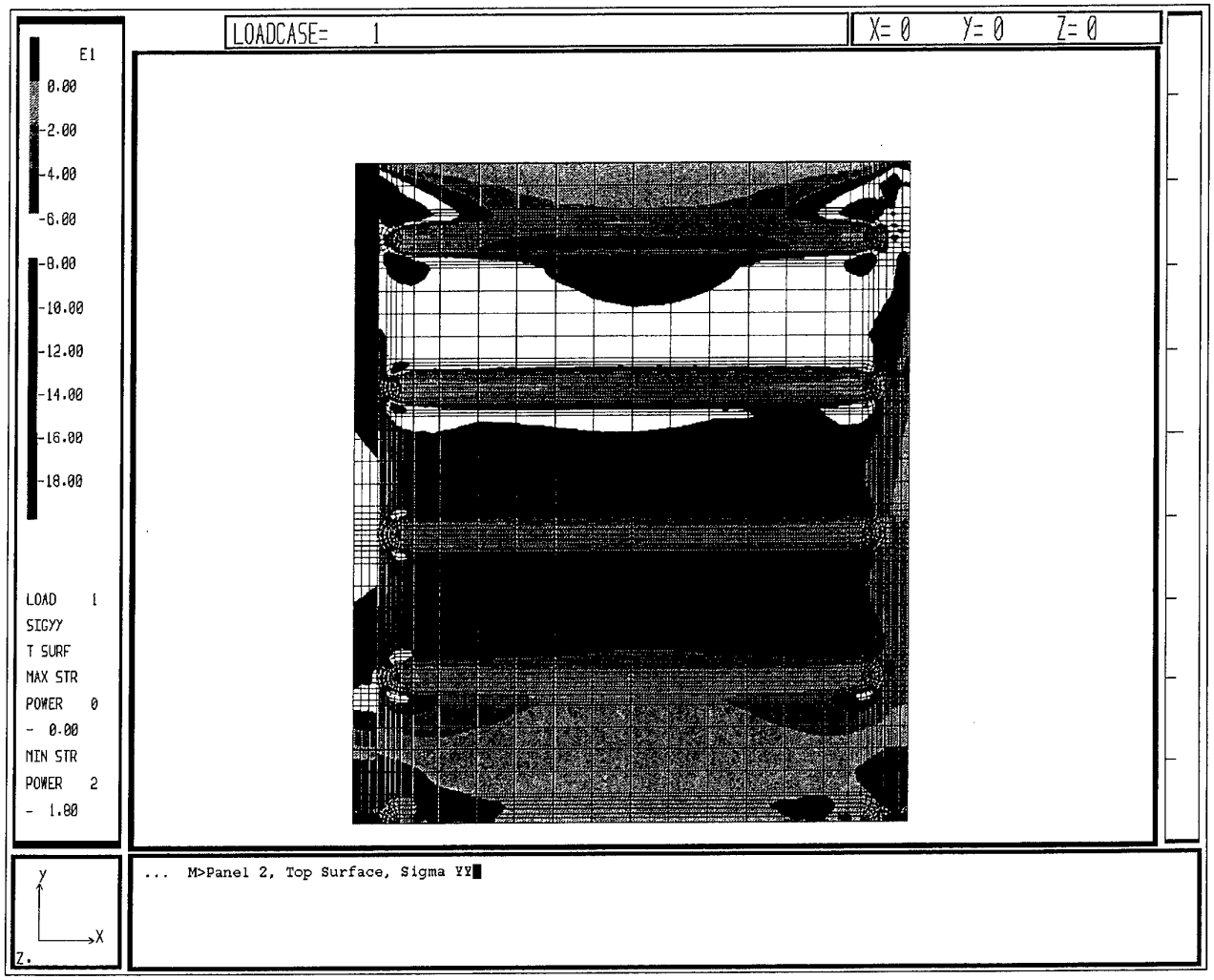

Figure F7. Panel 2 Top Surface sigma yy Stress

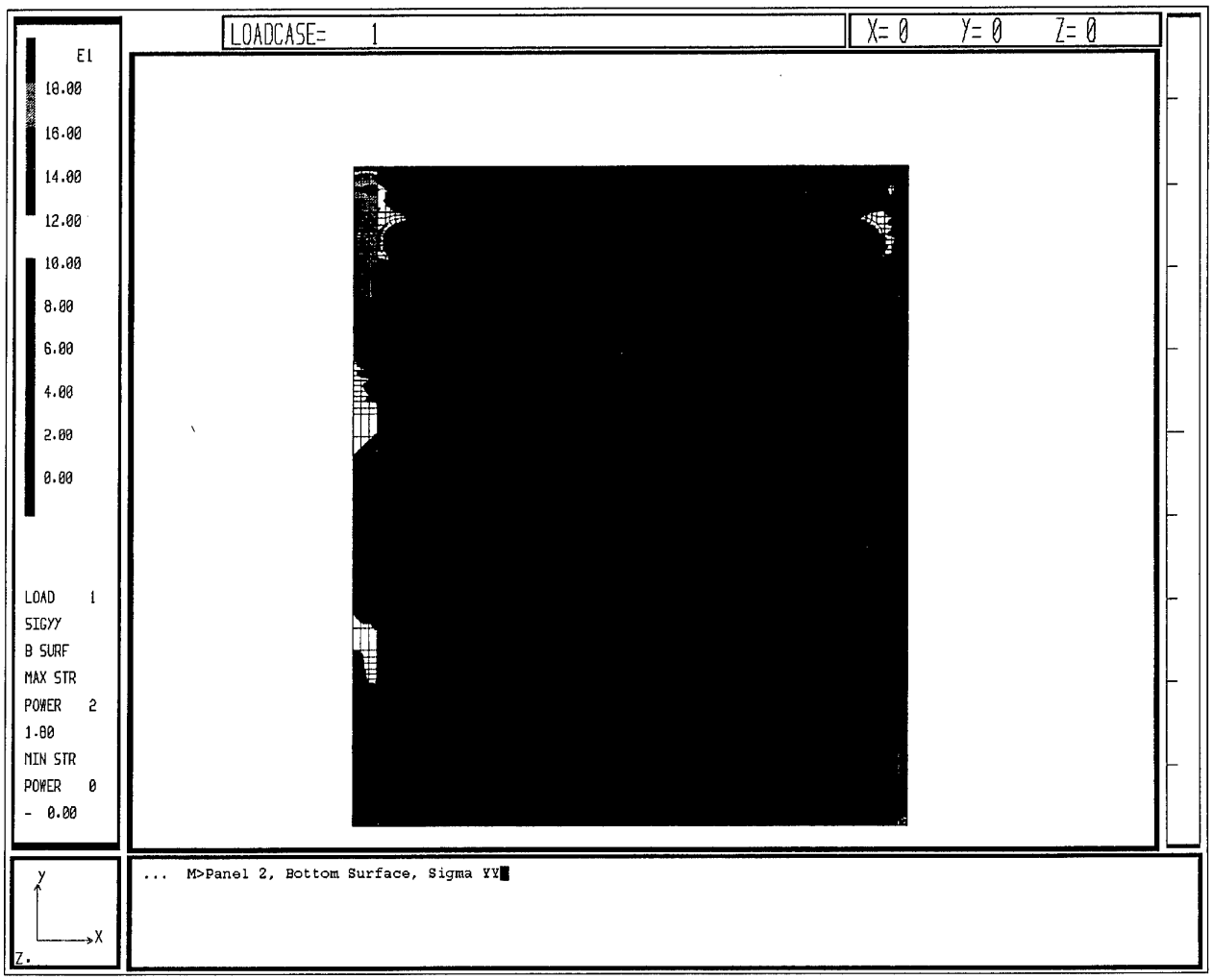

Figure F8. Panel 2 Bottom Surface sigma yy Stress

DISTRIBUTION LIST

Installation-Induced Stress in a Black Hawk Inner Fuselage Panel

C. G. Knight

AUSTRALIA

TASK SPONSOR:

DEFENCE ORGANISATION

Defence Science and Technology Organisation

Chief Defence Scientist
FAS Science Policy
AS Science Corporate Management
} shared copy
Counsellor Defence Science, London (Doc Data Sheet only)
Counsellor Defence Science, Washington
Senior Defence Scientific Adviser/ScientificAdviser Policy and Command (shared copy)

Aeronautical and Maritime Research Laboratory

Director
Chief of Airframes and Engines Division
TTCP HTP-8 Australian National Leader
K.F.Fraser
G. F. Forsyth
C.N.King
L.Krake
L.Molent
J.M.Grandage
D.C.Lombardo
S.A.Dutton
J.J.Paul
Author: C.G.Knight

DSTO Library

Library Fishermens Bend
Library Maribyrnong
Main Library DSTOS (2 copies)
Library, MOD, Pyrmont (Doc Data sheet)

Defence Central

OIC TRS, Defence Central Library
Officer in Charge, Document Exchange Centre (DEC), 9 copies
Defence Intelligence Organisation
Library, Defence Signals Directorate (Doc Data Sheet only)

Science Policy Division

Air Force Scientific Adviser
Scientific Adviser - Army
Staff Officer Science: Army HQ1 Divm.
Staff Officer Science: RAAF Base Townsville
Navy Scientific Adviser (3 copies Doc Data Sheet only)

Electronics and Surveillance Research Laboratory

Director
Library

Air Force

Army Aircraft Logistics Management Squadron:
Chief Engineer
Utility Helicopter Flight Commander
Black Hawk Logistics Manager
Aircraft Research and Development Unit:
WGCDR P. Campbell (CO Engineering Squadron)
Mr K. McCleod
SQNLDR D. Boorman
MAJ D. Fawcett
Director Technical Airworthiness
CAPT N. Skuja, AS12B, Army Aircraft Structural Integrity
Director Army Aircraft Projects
Technical Liaison Officer U.S. Army ATCOM (St Louis)
Technical Liaison Officer Warner Robbins Air Force Base (Georgia)

Army

Director of Aviation (Army)
Commanding Officer Maintenance Engineering Agency

Navy

Director Aircraft Engineering
Superintendent Aircraft Logistics

OTHER ORGANISATIONS

United Technologies Sikorsky Aircraft

T.J. Armond, S-70 ILS manager Worldwide Customer Services

U.S. Army

F.H. Immen, Head Engineering Structures and Materials Divn, U.S. Army ATCOM (St Louis, Missouri)
W. Elber, Director Vehicle Structures Directorate, NASA Langley Research Centre (Hampton, Virginia)
D.E. Good, Chief Air Vehicles Structures Division, Aviation Applied Technology Directorate (Ft Eustis, Virginia)

U.S. Navy

G. Barndt, Structures Branch, Naval Air Systems Command (Washington DC)

Chadwick Helmuth Company Inc.

L.L. Dobrin, Director of Business Development, On-Board Systems

VMS Inductries Pty Ltd

R. Mulder, Manager

SPARES (10 copies)
TOTAL (71)

DEFENCE SCIENCE AND TECHNOLOGY ORGANISATION
DOCUMENT CONTROL DATA

1. PRIVACY MARKING/CAVEAT (OF DOCUMENT)

2. TITLE

Installation-Induced Stress in a Black Hawk Inner Fuselage Panel

3. SECURITY CLASSIFICATION (FOR UNCLASSIFIED REPORTS THAT ARE LIMITED RELEASE USE (L) NEXT TO DOCUMENT CLASSIFICATION)

Document	(U)
Title	(U)
Abstract	(U)

4. AUTHOR(S)

C.G. Knight

5. CORPORATE AUTHOR

Aeronautical and Maritime Research Laboratory
PO Box 4331
Melbourne Vic 3001

6a. DSTO NUMBER	6b. AR NUMBER	6c. TYPE OF REPORT	7. DOCUMENT DATE
DSTO-TR-0329	AR-009-682	Technical Report	May 1996

8. FILE NUMBER	9. TASK NUMBER	10. TASK SPONSOR	11. NO. OF PAGES	12. NO. OF REFERENCES
M1/9/140	AIR 94/371	DTA-LSA	57	5

13. DOWNGRADING/DELIMITING INSTRUCTIONS

To be reviewed May 1999.

14. RELEASE AUTHORITY

Chief, Airframes and Engines Division

15. SECONDARY RELEASE STATEMENT OF THIS DOCUMENT

Approved for public release

OVERSEAS ENQUIRIES OUTSIDE STATED LIMITATIONS SHOULD BE REFERRED THROUGH DOCUMENT EXCHANGE CENTRE, DIS NETWORK OFFICE, DEPT OF DEFENCE, CAMPBELL PARK OFFICES, CANBERRA ACT 2600

16. DELIBERATE ANNOUNCEMENT

No limitations

17. CASUAL ANNOUNCEMENT Yes

18. DEFTEST DESCRIPTORS

Black Hawk helicopters; S-70A-9 Black Hawk; Fuselage skin; Cracking; Stress fracture; Stress fracture; Modelling

19. ABSTRACT

Some S-70A-9 Black Hawk helicopters of the Australian Army fleet are experiencing cracking on the starboard side internal fuselage skin panel. The panel is installed onto curved frames which causes installation-induced stresses in the panel. The PAFEC Finite Element package has been used to model the panel and to indicate the stresses and stress concentrations within it induced by the installation process.

The methods used for constructing and verifying the model are presented. The maximum stresses and stress concentration factors produced by the model are discussed.